UiT
THE ARCTIC UNIVERSITY OF NORWAY

FACULTY OF SCIENCE AND TECHNOLOGY

Department of Geology

Seabed depressions in the Ingøydjupet Trough and their relation to buried canyons on the Loppa High, Barents Sea

—

Richard Prytz

Master thesis in Energy, Climate and Environment.
June 2016

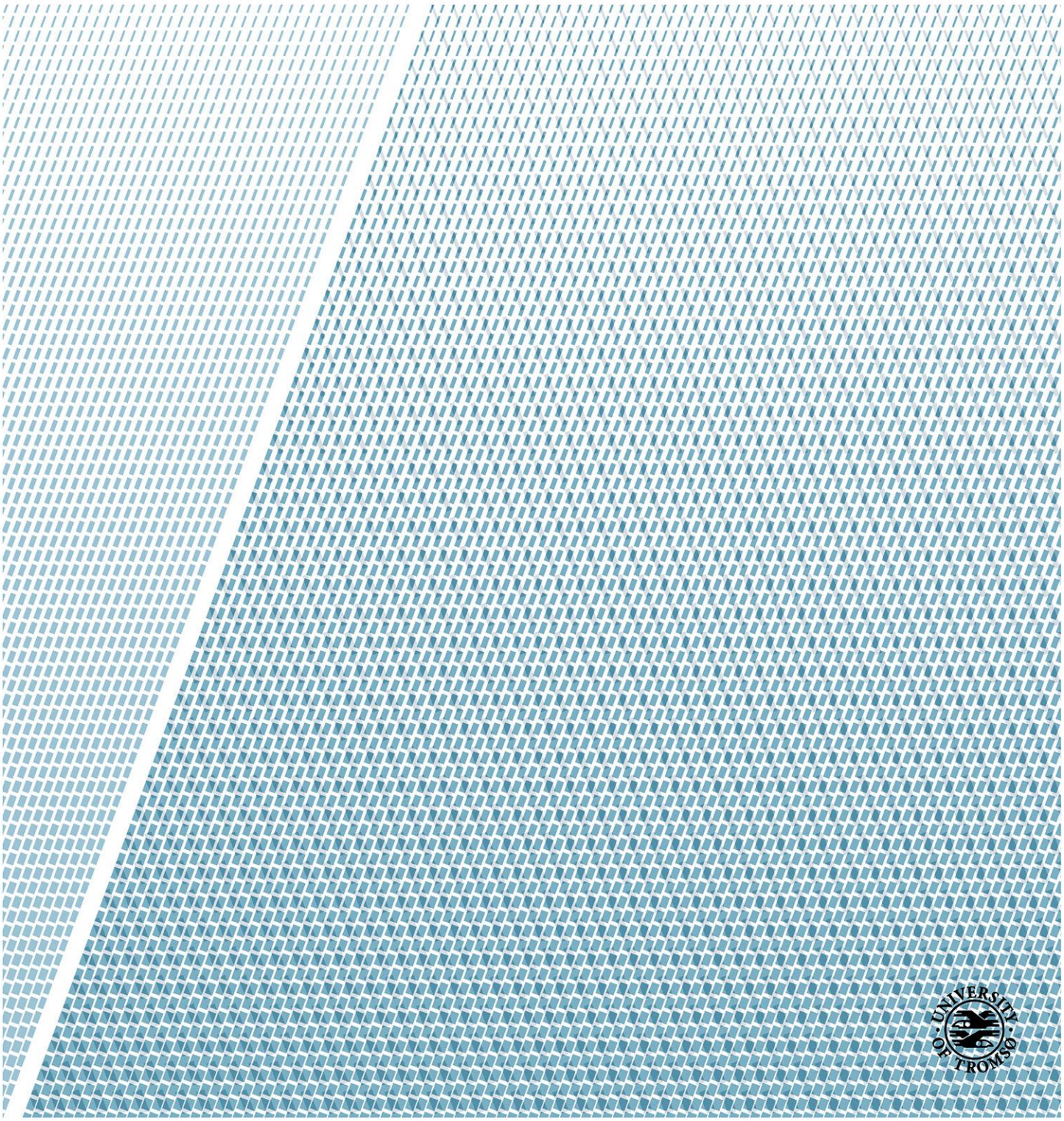

Abstract

Large seabed depressions in the Ingøydjupet Trough have previously been interpreted to be formed by sub-glacial melt-water. However, fluid migration and gas expulsion occur over large parts of the Barents Sea, which are frequently associated with seabed depressions. This thesis studies how the seabed depressions are related to sub-surface canyons on the southern part of the Loppa High, SW Barents Sea.

The canyons are located stratigraphically below the seabed depressions, and high-amplitude zones at the canyon crests indicate accumulation of gas. Migration of fluids seems to take place along the canyon flanks, and the canyons and their infills have been mapped out in order to infer the distribution of shallow gas and their relation to the seabed depressions.

Uplift and erosion have influenced the fluid flow system several times since the formation of the canyons. The final phase was related to glacial isostatic adjustment causing the gas to expand and build up pressure before eruption and seepage of shallow gas took place. Severe erosion further caused the seismic unit S2 to the absent in the southwestern parts of the study area. The thickness of S2 appears to affect the distribution of depressions and fluid migration, as it acts as an impermeable barrier where it is present and thus prevents fluids to reach the seabed and form depressions. The large seabed depressions above the canyons occur in areas where S2 is not present, which suggests that shallow gas is indeed a major contributor to the seafloor topography.

Acknowledgement

Masteroppgaven nærmer seg slutten, og 5 års studietid er plutselig forbi. Dette har vært en krevende, spennende og lærerik prosess.

Først og fremst vil jeg takke hovedveileder Tom Arne Rydningen, og biveiledere Jim Myrvang og Iver Martens for gode råd og kritikk. Setter virkelig pris på all hjelp og åpne kontorer.

Ønsker også å rette en stor takk til resten av EKM-kullet for mange trivelige stunder og et kjempeflott miljø. En stor takk må også rettes til andre medstudenter på brakka og ellers alle andre som har nytt godt av kontorets moccamaster.

En stor takk rettes også til mine foreldre for all støtte igjennom studietiden.

This research is partially funded by ARCEx partners and the Research Council of Norway (grant number 228107).

Richard Prytz

Juni 2016

Table of Contents

1 Introduction 1

1.1 Objective 1

1.2 Study area 2

1.3 Fluid migration 2

1.4 Acoustic fluid detection 3

1.5 Pockmarks 5

2 Geological background 7

2.1 Large-scale bathymetry of the south-western Barents Sea 7

2.3 Evolution of the south-western Barents Sea 7

2.3.1 Paleozoic 7

2.3.2 Mesozoic 8

2.3.3 Cenozoic 9

2.4 Mesozoic-Cenozoic stratigraphy and depositional environments 10

2.4.1 Mesozoic 10

2.4.2 Cenozoic 11

2.5 Structural elements 13

2.5.1 Loppa High 13

2.5.2 Hammerfest Basin 14

2.5.3 Bjarmeland Platform 15

2.6 Uplift and erosion of the Barents Sea – implication for hydrocarbon reservoirs 16

3 Data & methods 19

3.1 Datasets 19

3.1.1 Seismic data 19

3.1.2 Well data 21

3.2 Seismic interpretation and indications of fluids 21

3.3 Seismic Resolution 22

3.3.1 Vertical Resolution 23

3.3.2 Horizontal Resolution 23

3.4 Artefacts 25

3.5 Software 25

3.5.1 Petrel 25

3.5.2 CorelDraw 26

4 Seismic stratigraphy 27

4.1 Main reflectors 27

4.1.1 The base canyon reflector 27
4.1.1.1 Description 27
4.1.1.2 Interpretation 30
4.1.2 The URU: upper regional unconformity 30
4.1.2.1 Description 30
4.1.2.2 Interpretation 35
4.1.3 The seafloor reflector 35
4.1.3.1 Description 35
4.1.3.2 Interpretation 40
4.2 Seismic units 40
4.2.1 S0 40
4.2.1.1 Description 40
4.2.1.2 Interpretation 43
4.2.2 S1 43
4.2.2.1 Description 43
4.2.2.2 Interpretation 44
4.2.3 S2 47
4.2.3.1 Description 47
4.2.3.2 Interpretation 48
5. Discussion 49
5.1 Shallow gas accumulations on the southeastern Loppa High 49
5.1.1 Source and migration of fluids 49
5.1.2 Distribution of shallow gas 51
5.2 Large collapse features and pockmarks on the seabed and URU 53
5.3 Historical evolution and its impact on the observed depressions 56
6. Conclusion 59
7. References 61

1 Introduction

1.1 Objective

The objective of this thesis is to explain and document how large seabed depressions occur in the distal parts of the Ingøydjupet Trough, SW Barents Sea (Figure 1-1), with the aim of connecting these to sub-surface fluid migration. Earlier studies shows that fluid flow occur over large parts of the Barents Sea, and depressions (e.g. pockmarks) are frequently associated with accumulation of gas and fluid expulsion (e.g. Chand et al., 2012; Vadakkepuliyambatta et al., 2013). The depressions seen in Ingjøydjupet have previosly been interpreted to be tunnel valleys formed by sub-glacial melt water (Andreassen et al., 2008). However, there are canyons located stratigraphically below these seabed depressions, and there seems to be a strong correlation between the canyons, depressions, fluid migration and accumulation. This thesis will investigate the distribution of shallow gas and high-amplitude anomalies in order to document the correlation between the canyons and seabed depressions. This is done by interpretating the 3D seismic survey SG9803 with the use of geophysical attributes.

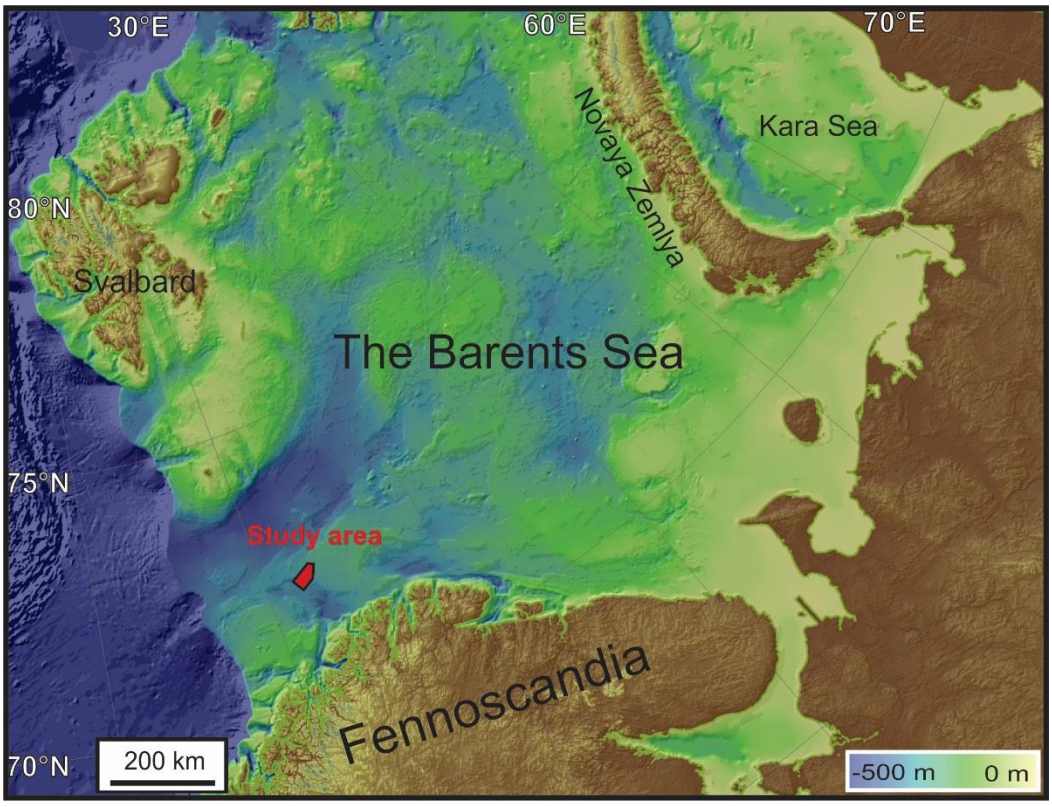

Figure 1-1: Bathymetric map of the SW Barents Sea and its surroundings. The location of the study area is indicated in red.

1.2 Study area

The study area for this thesis covers about 850 km^2 and is positioned between 71°53'-72°18 N 22°00' - 23°31' E at a maximum water depth of 400 m. The area is situated within Ingøydjupet Trough in the SW Barents Sea, a 150 km long glacial trough located north of Sørøya between Nordkappbanken and Tromsøflaket. Structurally, the study area is located on the southern part of the Loppa High, bordering the Bjarmeland Platform and the Hammerfest Basin.

1.3 Fluid migration

Subsurface fluid forces are governed by gradients found in excess water pressure, natural buoyancy temperature, and capillarity pressure differences. Lithologic layers slow or restrict the vertical movement of hydrocarbons (Hooper, 1991). However, migration pathways do not always enable fluids to reach the seabed; hence, accumulation of shallow gas may take place (Judd, 2004).

The fact that faults may act as both conduit and seal for fluids is well known, and may contribute to migration pathways (Wiprut & Zoback, 2000; Cartwright et al., 2007). Faulting, in general, will reduce porosity and permeability because of crushing and grinding of grains within sediments. Cementation of faults may cause sealing of faults, which in turn stops migration. As fluid migration is halted, pressure will begin to build up. If the pressure exceeds the fracturing pressure, further faulting will take place. This process may repeat itself and cause interference within the migration pathways (Knipe, 1992). At the sides of fault zones, hydrocarbons may migrate into permeable strata and appear as bright spot. This might be challenging to identify in seismic due to uneven distribution and undefined fault zones. Variations of leakage anomalies within leakage zones are classified as: stratigraphic levels where the gas chimney terminates; levels dominated by high amplitudes; or the top of mobilized sediments. Several leakage processes may take place within one leakage zone (Løseth et al., 2008).

Permeability (k) is a rock property and the measurement of the ability of a porous material to allow fluids to pass through it. Permeability is governed by Darcy's law (Eq 1.1), which relates discharge and fluid physical properties to a pressure gradient applied to the porous rock. Other contributing factors

is shapes of the pores in the rock and their level of connectedness, such as level of sorting and consolidation (Bear, 1972).

$$Q = \frac{-k\,A\,(P_2 - P_1)}{\mu\,L} \qquad \text{Eq 1.1}$$

Q = Fluid flux (m^3/s k = Permeability (m^2) A = Area (m^2)

μ = Viscosity (Pa · s) L = Migration length (m) P_2-P_1 = ΔP = Pressure difference (Pa)

Equation 1.1 is only valid if there is an absence of chemical reactions, single fluid phase, and constant elevation, constant instantaneous discharge rate through the rock and viscosity (Bear, 1972; Whitaker, 1986).

As differential pressures, (ΔP) increases with depths, the density and porosity will decrease monotonically due to overburden. Compaction will cause an imposing force on grain contacts, which causes shift and rotation of grains, it is highly dependent on lithology and diagenetic processes, such as cementation fill in pore spaces. Although overburden, in general, increases density, it might have a positive effect on porosity and fluid flow as rocks fractures (Guzzetta & Cinquegrana, 1987; Castagna et al., 1993; Berndt, 2005) .

1.4 Acoustic fluid detection

Seismic expressions of fluid flow are often recognized by high amplitude anomalies and commonly an indication of hydrocarbon pathways. These indicators may show both increase and decrease in acoustic impedance. These features include seepage pipes, pockmarks, acoustic pull downs related to fluid migration, and bottom-simulating reflectors (BSR) (Andreassen et al., 2007; Vadakkepuliyambatta et al., 2013).

Vertical migration of gas through subsurface strata can cause widely distributed acoustic low-velocity zones, called acoustic masking (Fig 1.2 a), and is often linked to shallow gas accumulations. Acoustic

masking is a result of deterioration of the seismic data and causes regions of chaotic signals. The nature and shape of these zones varies accordingly with the process of geological formation, and are commonly observed with most types of sediment mobilizations (Vadakkepuliyambatta et al., 2013). Pull down effect (Fig 1.2 a) is a result of low velocity zones caused by gas within sediments. The presence of gas causes a severe decreases in P wave velocity, thus the reflection will appear deeper in the seismic than it actually is. (Judd & Hovland, 2007; Andreassen et al., 2007).

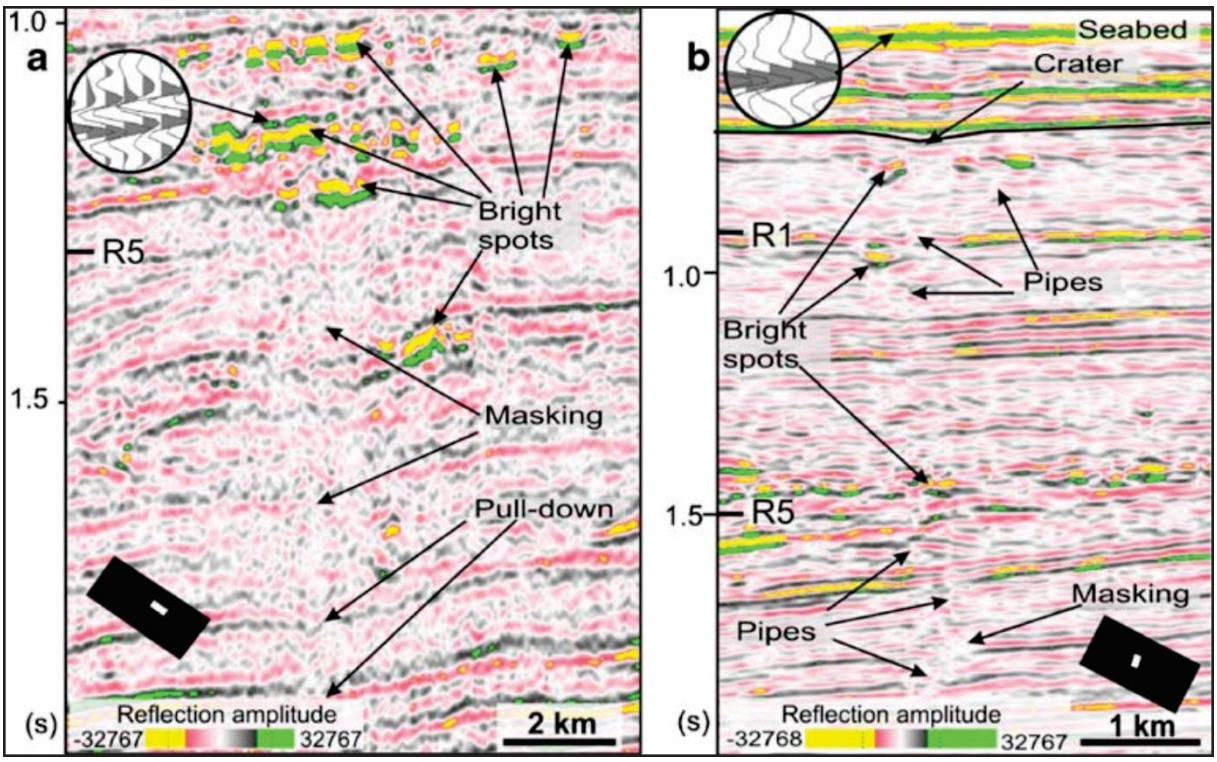

Figure 1.2 – A seismic profile showing different types of seismic indications of fluids associated with fluid flow. From (Andreassen et al., 2007).

1.5 Pockmarks

Pockmarks are a circular to elongated crater-like depressions found on the seabed caused by fluids erupting and streaming through the sediments (Figure 1-3) (Hovland & Judd, 1988). The pockmark density varies greatly from area to area and may reach up to 60 per km^2 in Norwegian offshore areas (counting only those with a diameter of 10 m or more). Size is also a fluctuating parameter, and their diameter are generally between 50 and 100 m with depths in the range of 1-3 m (Judd & Hovland, 2007).

Pockmarks are generally accepted as morphological expressions of leakage from subsurface petroleum systems and in most cases attributed to expulsion of gas and pore fluids from underlying sedimentary rocks or sediments (hydraulically active areas). Exploration geologists use pockmarks as a guide in hydrocarbon exploration and in seismic, they are often located above zones of acoustic masking, such as gas pipes and gas chimneys. They can be an indication of fluid flow and gas hydrate accumulation (Figure 1-3). Features associated with seeps can be easier to identify than seabed seepages by themselves (Judd & Hovland, 2007; Chand et al., 2012; Vadakkepuliyambatta et al., 2013; Rise et al., 2015).

The SW Barents Sea region, including the western flank of the Loppa High and the Hammerfest Basin, is also home to many relict pockmarks. These pockmarks are interpreted to have formed by methane released due to gas hydrate dissociation during the last deglaciation. The largest pockmarks usually occur in the deepest parts of the troughs where postglacial clays are thickest and decreases towards basin flanks (Rise et al., 2015).

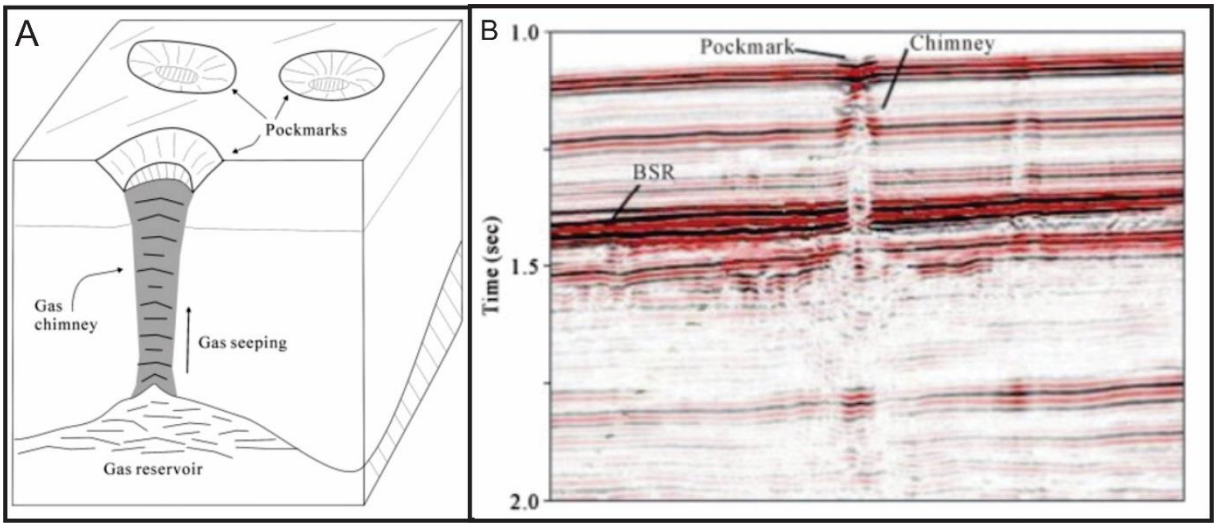

*Figure 1-3: **A**: Concept model of a pockmark depression. Gas discharge from the reservoir through a gas chimney. From Hovland (1989). **B**: A seismic profile of the occurrence of a pockmark. From Cathles et al. (2010).*

2 Geological background

2.1 Large-scale bathymetry of the south-western Barents Sea

The Barents Sea is a shallow, sub-arctic marginal sea located off the northern coast of Norway and Russia. It borders the Norwegian Sea to the west, Svalbard to the north-west, Franz Josef Land to the northeast, Novaya Zemlya to the east, the Kola Peninsula to the south and the Polar Sea to the North. The Barents Sea spans 1 400 000 km^2 with the vast majority in the Russian territorial waters. As the majority of the sea is located on the shelf, the average depth varies between 200 to 500 meters (Doré, 1995; Hoel, 2016). The Barents Sea is an epi-continental sea, making the present shelf area one of the widest continental shelves in the world. The topography is partly influenced by the underlying bedrock and structural trends, and it is rather irregular and characterized by several shallow bank areas. The mouths of some of the troughs also display large submarine fans. Other prominent large-scale features on the continental shelf are wedges, mega scale glacial lineations and iceberg scouring, which is caused by the ice flows from the decay of the Fennoscandian ice sheet during the Last Glacial Maximum (LGM) (Andreassen et al., 2008).

2.3 Evolution of the south-western Barents Sea

The Barents Sea has an extensive and complex history, which is related to erosion, uplift and subsidence, and may be divided into 3 dominant rift phases: The Late Devonian-Carboniferous, the Middle Jurassic – early Cretaceous, and the early Cenozoic. A number of tectonic pulses are found in each phase as well (Faleide et al., 2015).

2.3.1 Paleozoic

During late Paleozoic, crustal extension took place in most of the area. This extension is characterized by a general westward migration of the rifting formations that has caused well-defined rifts and basins. The crustal extension also caused strike slip fault development in the northern areas. The area has been largely stable since Late Paleozoic times, with the exception of epeirogenic movement that has caused most of today's vertical seabed levels. (Faleide et al., 1993). The SW Barents shelf was formed

as a central part of the northern Late Devonian Pangean margin, which is underlain by a Devonian metamorphic basement that did form during the Caledonian Orogeny that provided a structural framework for this area (Worsley, 2008; Smelror et al., 2009).

As the crustal expansion during the Carboniferous took place in most of the Barents Sea, half graben features began to develop with a NE-trend that can be seen as the Hammerfest Basin today. The Loppa and Stappen highs were also subject to heavy faulting during the Late Carboniferous to early Permian, while northeastern parts of the Bjarmeland Platform and Nordkapp Basin were stable (Riis et al., 1986; Worsley, 2008). Climate change during the Carboniferous also took place that caused extensive evaporite depositions in the deepest basins (Smelror et al., 2009).

2.3.2 Mesozoic

During the Paleozoic-Mesozoic transition, extensional tectonic movements took place that dominates the Paleozoic and Mesozoic tectonic history. These tectonic movements also triggered fault movements that affected the region. (Faleide et al., 1993). Tectonic activities were most active during the Mesozoic and Cenozoic times in the western parts of the Barents Sea and activity levels began to cease towards the Triassic and early Jurassic. However, reactivated rifting began to take place during the Triassic, which caused tilting of the Loppa and Stappen highs (Gudlaugsson et al., 1998). The eastern areas were also subject to regional subsidence and influx of sedimentations during the early Triassic (Gudlaugsson et al., 1998; Worsley, 2008).

The Mid-Jurassic is characterized by rifting and extensional block faulting, which is related to the opening of the Central Atlantic. This Atlantic rifting began to accelerate during the Late Jurassic towards the Cretaceous and as the North Atlantic opened, major basins and highs ceased to develop (Faleide et al., 1993). Faulting with eastern and northeastern trends also took place during the Mid-Jurassic due to the onset of the Kimmerian tectonic phase. This tectonic stage caused extension and strike-slip alterations, which further sparked sea level changes and a regional transgression. Shales began to deposit and further subsidence of the Harstad, Tromsø and Bjørnøya basins took place and became major depocenters, as well with doming in the Hammerfest Basin, and other features such as the Loppa fault complex (Faleide et al., 1984; Faleide et al., 1993; Worsley, 2008). Uplift and erosion of the northeastern parts of the Barents Sea brought sediments in these depocenters (Smelror et al., 2009).

In the early Cretaceous, rifting of the Atlantic continued to play a major role and several pull-apart basins formed (Figure 2-2), such as Sørvestsnaget Basin and the Vestbakken Volcanic Province (Smelror et al., 2009). There are at least three tectonic phases related to Atlantic rifting during the Cretaceous, which had a profound effect on the marginal structure, which is characterized by extension along the Bjørnøyrenna fault complex, and terminated rifting in the Hammerfest Basin. The Loppa fault complex were also given a further activation in the northwestern plane as the Atlantic rifted northwards. (Faleide et al., 1993). During the Cretaceous, Loppa High was an island that eventually became inverted as it subsided between the Bjørnøy and Hammerfest basin. Kimmerian fault movements also began to cease (Faleide et al., 1984). In the Late Cretaceous Atlantic rifting of Norway and Greenland continued but changed towards a strike-slip movement. The western basins began to subside, while eastern areas experienced uplift (Faleide et al., 1984; Smelror et al., 2009).

2.3.3 Cenozoic

Strike-slip movement prevailed in the Cenozoic that caused further deformations (Smelror et al., 2009). These deformations lead to the formations of additional pull-apart basins in the western parts of the Barents Sea (Faleide et al., 1993). The rifting eventually changed towards a NW-SE course that induced a reactivation of faults in the Vestbakken Volcanic Province and embryonic seafloor spreading and graben formations took place around Svalbard (Smelror et al., 2009). Paleocene depositions took place in these deep marine conditions and persisted today as features such as submarine fans the Sørvestsnaget basin (Ryseth et al., 2003). Separation of the Barents Sea shelf and Greenland Sea as continued since the Oligocene and crust has been formed along the whole margin of the Barents Sea. This crust formation further causes subsidence and accumulation of a thick Late Cenozoic sedimentary wedge, which is fed from erosional processes from the Barents Shelf and Svalbard area (Faleide et al., 1996).

The marginal evolution of the SW Barents Sea, as a passive shear margin, is closely linked to the successive northward opening of the Norwegian-Greenland Sea, which began in the Paleocene-Eocene transition. The history, is however, rather complex and uncertainties are linked to the area around the opening of the southern Greenland Sea. Magnetic anomalies constrains the areas around Senja fracture zone. The Greenland Sea is further extended in the northern areas due to alterations of the spreading directions (Faleide et al., 1996).

Glaciation and deglaciation in the Northern Hemisphere has had a major effect on the Barents Sea, which has been subjected to glaciation on several occasions during the Late Cenozoic. In addition to

glaciation, uplift took place as well and the entire Barents Shelf was uplifted during one phase. Because of this, severe erosion occurred and large amounts of sediments were deposited along the western margin (Nyland et al., 1992). Notably large sediment accumulations are found west of Bjørnøya, dominated by trough mouth fans, where packages formed in very thick layers of glacigenic origins (Vorren et al., 1991). Southern parts of the southwestern parts, such as the Hammerfest Basin and Loppa High, were subjected a lesser amount of uplift and erosion, usually experiencing less than 2 km of erosion (Smelror et al., 2009; Henriksen et al., 2011 b).

2.4 Mesozoic-Cenozoic stratigraphy and depositional environments

2.4.1 Mesozoic

During the Triassic, the Barents Sea experienced a deceasing trend in tectonic activities, and remained rather stable. Although regional subsidence took place (Smelror et al., 2009). Non-siliceous fine clastics were dominating in early-mid Triassic. As for highs and platforms, there is a major hiatus during the transition between Permian and Triassic times. Southwestern areas were also prone to coastal sedimentation with sources from the Fennoscandian Shield and the Uralian orogeny, which also played a role on sediment transport to deep basins. (Worsley, 2008). The time span of Mid-Triassic to Late Triassic, shallow shelf depositional environments generally display alternating marine transgression and regression events. A major sea level rise towards the Jurassic combined with uplifting and high sedimentation rates, eventually led a vast marine shelf foundation in the Barents Sea. (Faleide et al., 1984). The Late Triassic-Early Jurassic also displays deltaic and fluvial settings, which reached Svalbard, and large areas were prone to erosion through uplifting. Flooding of shallow marine environments also took place in western parts, resulting in anoxic conditions and the formation of anoxic basins (Smelror et al., 2009). Early and Middle-Jurassic is characterized by areas of uplift and erosional processes in the western parts of the Barents shelf, which, during the Early Cretaceous, spawned a major sandstone layer amongst the western margins of the Barents Sea as a result of a Late Jurassic Early Cretaceous rift phase. This sandstone layer is a prominent upper part of present Loppa High and Hammerfest basin. Distal and open areas went through development of claystones (Smelror et al., 2009). Fault-controlled subsidence took place in areas towards Svalbard, which consists narrow extensional basins containing marginal continental red beds that passes laterally into basinal carbonates and evaporites (Steel & Worsley, 1984). Late Cretaceous suffers from a heavy hiatus in its seismic data in the Barents areas (Faleide et al., 1984).

2.4.2 Cenozoic

The onset of the Paleocene is characterized by severe flooding patterns in elevated areas, such as the Loppa High, due to a major marine transgression event. Subsidence related depositions took place in basins eastward from the Loppa High. Indications of a regional hiatus is also present (Clark et al., 2014). The Paleocene succession indicates an uplift of the wider Barents platform, relative to the Tromsø and Bjørnøya basins (Worsely et al., 1988).

From Late Cenozoic times to present, uplift and erosion were dominating events, as were fluctuating quaternary glaciations that specifically began to shape the recent geological history. This led to thick and prograding sedimentary depositions into the oceanic basins to the west and north (Faleide et al., 1996). Uplift and glacial erosion has led to limited distribution of Cenozoic strata with estimates of net erosions that exceeds as much as 500 m in several areas (Nyland et al., 1992).

Glacial packages fluctuates between 0-300 m in thickness on areas on the shelf, and 900 – 1000 m on areas found on the shelf break (Vorren et al., 1991; Andreassen et al., 2008). As the ice sheet retreated, depositions of silt and clay mixed with ice rafted debris. This continued for thousands of years and eventually left glaciomarine clays, which is thickest in depressions and low-lying areas that reach up to 15 m in Ingøydjupet (Chistyakova et al., 2010). Large morphological features are seen on the seabed, which illustrates the dynamic actions of the retreating ice sheet (Andreassen et al., 2008; Winsborrow et al., 2010).

East of Bjørnøya, glacial deposits can be distinguished from the underlying bedrock from a major seismic reflector, which is the Upper Regional Unconformity (URU) that diverges into several unconformities (Vorren et al., 1991; Laberg et al., 2012). In southeastern parts of the Barents Sea, the URU is sub-parallel with the seafloor and exhibits a horizontal trend, but lowers horizontally westwards (Andreassen et al., 2008).

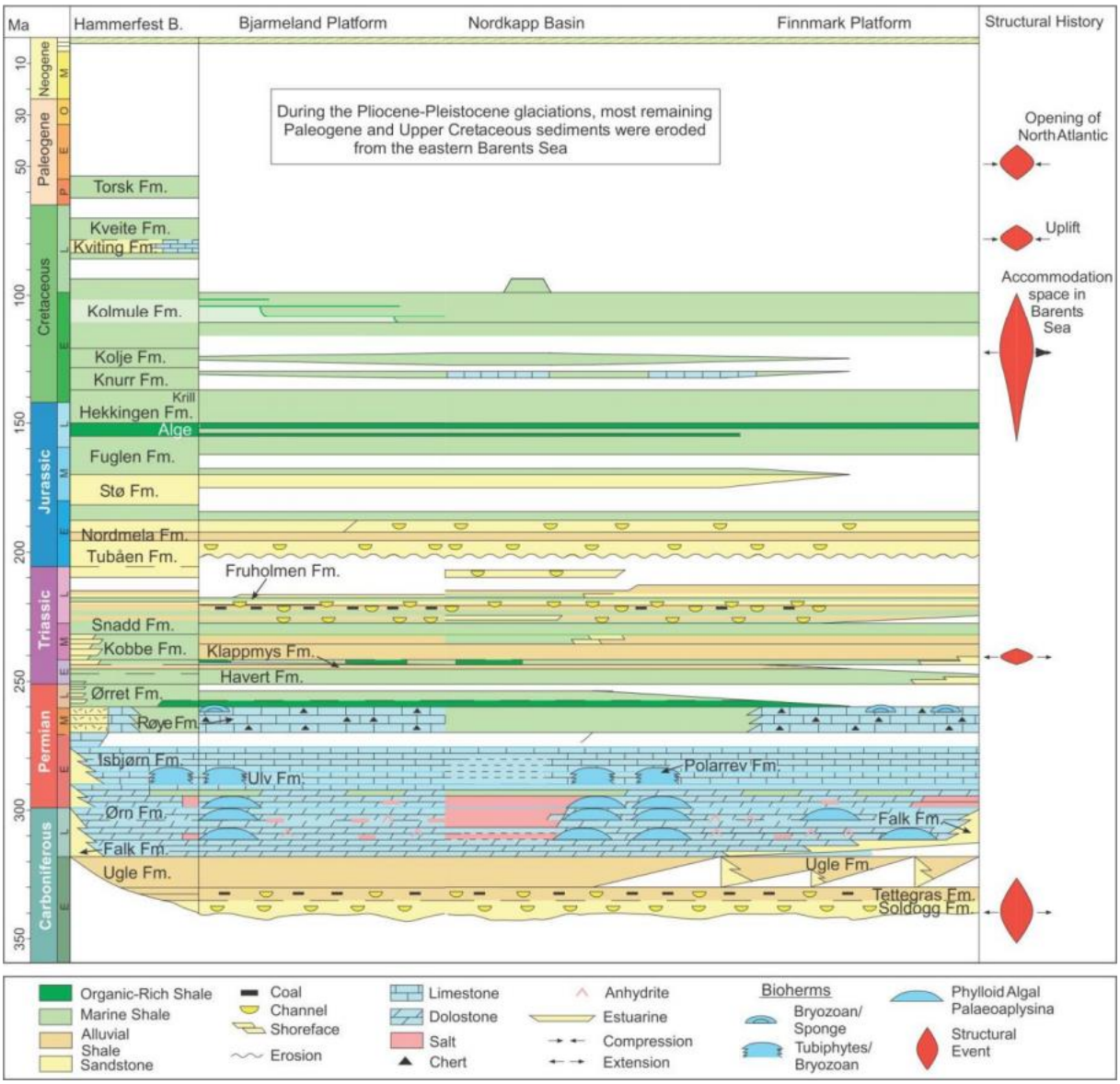

Figure 2-1: Lithostratigraphic diagram of the SW Barents Sea from the Triassic to present day. From (Ohm et al, 2008).

2.5 Structural elements

The western Barents Sea and Svalbard continental margin consist of structures that can be separated into three regions: A southern sheared margin along the Senja fracture zone, a central rift complex associated with volcanism and a northern initially sheared, and later rifted, margin along the Hornsund fault zone. The Senja Fracture zone, along with Vestbakken Volcanic Province, imprints the western limit of the shelf and the transition to oceanic crust. The fault systems of Bjørnøyrenna and Ringvassløy-Loppa are used to define the limit boundaries between eastern and western parts of the southwestern Barents Sea and it is bound to the Loppa High in the west (Faleide et al., 1984; Halland et al., 2013). The western areas of the Barents Sea also includes Jurassic-Cretaceous fault zones that forms some deep sedimentary basin boundaries (Faleide et al., 1984).

2.5.1 Loppa High

The Loppa High is situated north of the Hammerfest Basin and southeast of Bjørnøya Basin (Fig 2-2). The Loppa High consists of an eastern platform and crestal western and northwestern margin and possesses a diamond shaped outline. It is separated in the south by the east-western trending Asterias Fault Complex. To the west, it is separated from the Tromsø and Bjørnøya Basins by the Ringvassøy-Loppa and Bjørnøyrenna Fault complexes. In The east and southeast, it borders as a monocline fold towards the Bjarmeland Platform and the Hammerfest Basin. The northeastern border is marked by a major salt structure, the Svalis Dome, and its associated rim syncline, the Maud Basin. It is associated with positive gravity and magnetic anomalies caused by a relatively shallow metamorphic basement of Caledonian age, which underlie its western parts (Gabrielsen et al., 1990).

The western crest has been rejuvenated as a high at least four times since the Devonian, but tectonism during Late Jurassic to Early Cretaceous and Late Cretaceous-Tertiary defined its present outline (Gabrielsen et al., 1990). An important part of the erosional process took place in the Quaternary when erosion rates increased due to the glacial conditions (Halland et al., 2013).

The Loppa High exhibits a complex geological history with several phases of uplift and subsidence followed by tilting and erosion. During the Late Carboniferous, rift topography was filled an overlain by Upper Paleozoic siliclastics, evaporites and carbonate. In the Late Permian to Early Triassic, the Loppa Ridge was uplifted and tilted, followed by a gradual onlap during the Early and Middle Triassic.

A deposition of thick Upper Triassic layer formed which is now known as the Snadd Formation. On the southern crest, Paleogene shales formed and overlies Middle Triassic claystones (Halland et al., 2013). The Loppa High exhibits a Polygonal Reef Pattern due to fluctuating sea-level changes caused by up to 100 m thick algae build-ups (Smelror et al., 2009).

2.5.2 Hammerfest Basin

The Hammerfest Basin (Fig 2-2), a shallow basin with depths up to 6-7 km with an ENE-WSW striking axis, is separated from the Finnmark Platform to the south by the Troms Finnmark Fault Complex, and from the Loppa High to the north by the Asterias fault Complex. Its western limitation towards the Tromsø Basin is defined by the southern segment of the Ringvassøy-Loppa High Complex, whereas its eastern border at the reference level has the nature of a lithospheric flexure against the Bjarmeland Platform (Gabrielsen et al., 1990). The eastern and northern border faults juxtapose a Jurassic aquifer towards Triassic formations. Eastern parts exhibits gradual transitions into formations found in the Bjarmeland Platform (Halland et al., 2013). The Hammerfest Basin may be parted into two sub-basins – western and eastern, which is diverged by the extension of the Trollfjord-Komagelv fault trend. The western sub-basin show a generally westward trend towards the Tromsø Basin and is characterized by a moderate central dome, which parallels the basin axis. Its fault system show trends in the E-W, ENE-WSW and WNW-ESE directions. As for the eastern sub-basin, it shows lesser trends of faulting, and it exhibits sag basin characteristics. Structurally, the Hammerfest Basin has been dominated by extension, although it has been suggested that the deformational style indicates Late Jurassic to Early Cretaceous strike-slip reactivation (Gabrielsen et al., 1990).

Northeastern trending basins of the southern Barents Sea can be traced back to Late Devonian to Early Carboniferous times, which is pursuant with the separation dates of the Hammerfest Basin from the Finnmark Platform that occurred in Late Carboniferous times. The Hammerfest and Tromsø basins were presumably parts of a larger epeirogenic depositional system during the Triassic to Early Jurassic, still it appears as the Hammerfest Basin identified as a separate depocenter during the Lower Triassic. The present outlines emerged during the Mid Jurassic, along with its central dome feature (Gabrielsen et al., 1990).

The strata of Middle to Upper Triassic is characterized by lower sequences of interbedded shales and sandstones, which is periodically carbonaceous with fragments of coal, overlain by a shaly and silty unit that with an increasing amount of sandstone upwards. Sediments are interpreted to be of deltaic environments (Linjordet & Grung, 1992). From Lower to Middle Jurassic, the strata consists primary of

sandstones interbedded with thin shale layers. These layers are deposited in a shallow marine to coastal plain environment with fluctuating coastlines (Linjordet & Grung, 1992).

2.5.3 Bjarmeland Platform

The Bjarmeland Platform (Fig 2-2) is situated, and represents, the area between the Hammerfest and Nordkapp basins to the south and southeast, and against Sentralbanken and Gardarbanken highs in the north. It borders, and is terminated by, the crestal areas of Loppa High in its southwestern areas. The Bjarmeland platform went through an uplift during the Tertiary, which resulted a gently southerly dip of platform sediments and a gradual subcrop of older sediments to the north at the unconformity of the Quaternary base (Gabrielsen et al., 1990). Stable Late Paleozoic structural features are found in the Bjarmeland Platform. These structural features are interpreted as a transition from a pre-platform to a platform development during boundary between Early Carboniferous clastic rocks and Late Carboniferous to Permian carbonates. Foraminifera found in cores indicates similar results (Gabrielsen et al., 1990; Bugge et al., 1995; Larssen et al., 2002).

The platform started to develop as a stable platform during the Late Carboniferous, and is assumed to be underlain by Paleozoic and Precambrian rocks. It was presumably terminated to the west by a fault zone, with a north-south orientation, during the Late Permian to Early Triassic. Its border against Loppa High took place as a result of tectonism during Late Mesozoic, which gave rise to the present Loppa High and Fingerdjupet subbasin. Structural elements in central areas of the Bjarmeland platform are related to salt tectonics and fragile extension (Gabrielsen et al., 1990).

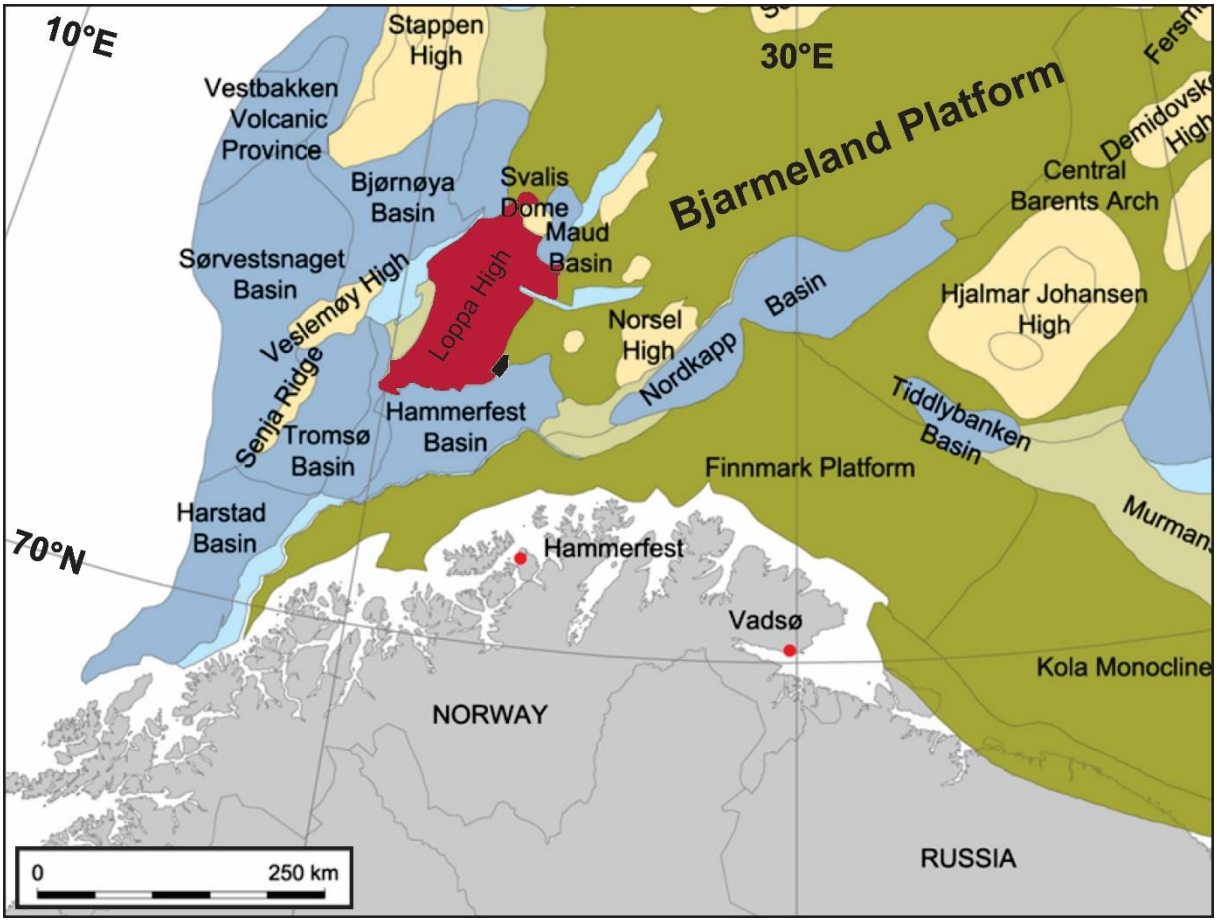

Figure 2-2: Structural elements in the study area. Loppa High shown in red. Seismic survey SG9803 shown in black. Modified from (Henriksen et al., 2011).

2.6 Uplift and erosion of the Barents Sea – implication for hydrocarbon reservoirs

Uplift and erosion has taken place in the southwestern Barents Sea on several occasions. Different methods, such as vitrinite reflectance, fission track analysis and mass balance calculations, shows a range between 500 and 3000 m, with an increase from west to east (Figure 2-3). It is important to distinguish between tectonic uplift, which is an active uplift mechanism, and passive uplift caused by erosion of sediments that leads to isostatic adjustment. Active uplift mechanisms leads to erosion and place sediments above sea level (Reemst & Cloetingh, 1994). The south-west Barents Sea also exhibits deformed sequencing due to tectonic movements from the Late Mesozoic and Cenozoic, which differs from the thick and un-deformed general trend in the Barents Sea. This has proven to make structural correlations difficult task (Nyland et al., 1992). This large-scale, predominantly glacially related, uplift

and erosion that has caused a major impact on sedimentation depositions and other features such as hydrocarbon accumulation in petroleum systems. As for prospectivity, the reservoir qualities, at certain depths, are generally lower than expected and source rocks display more maturity than expected. A majority of Barents Sea wells shows that most the Paleogene section and the entire Neogene section is not present (Henriksen et al., 2011 b). Seal failure related to removal of sedimentary overburden is thought to be the primary cause of such reservoir properties. Other reservoir qualities affected by uplift are porosity and permeability. Reservoir rocks tend to have the compaction and diagenetic properties that reflects its deepest burial depth. However, diagenetic processes will in general reduce porosity and permeability, causing the uplifted reservoir rock to possess a lower reservoir quality than expected at this depth (Doré & Jensen, 1996).

Reduced pressure related to uplift and erosion will cause present gas to expand. Hence, if a reservoir is filled to its spill point, the hydrocarbons will eventually leak out from the reservoir. In other words, present oil will leak out, essentially leaving only gas (Doré, 1995).

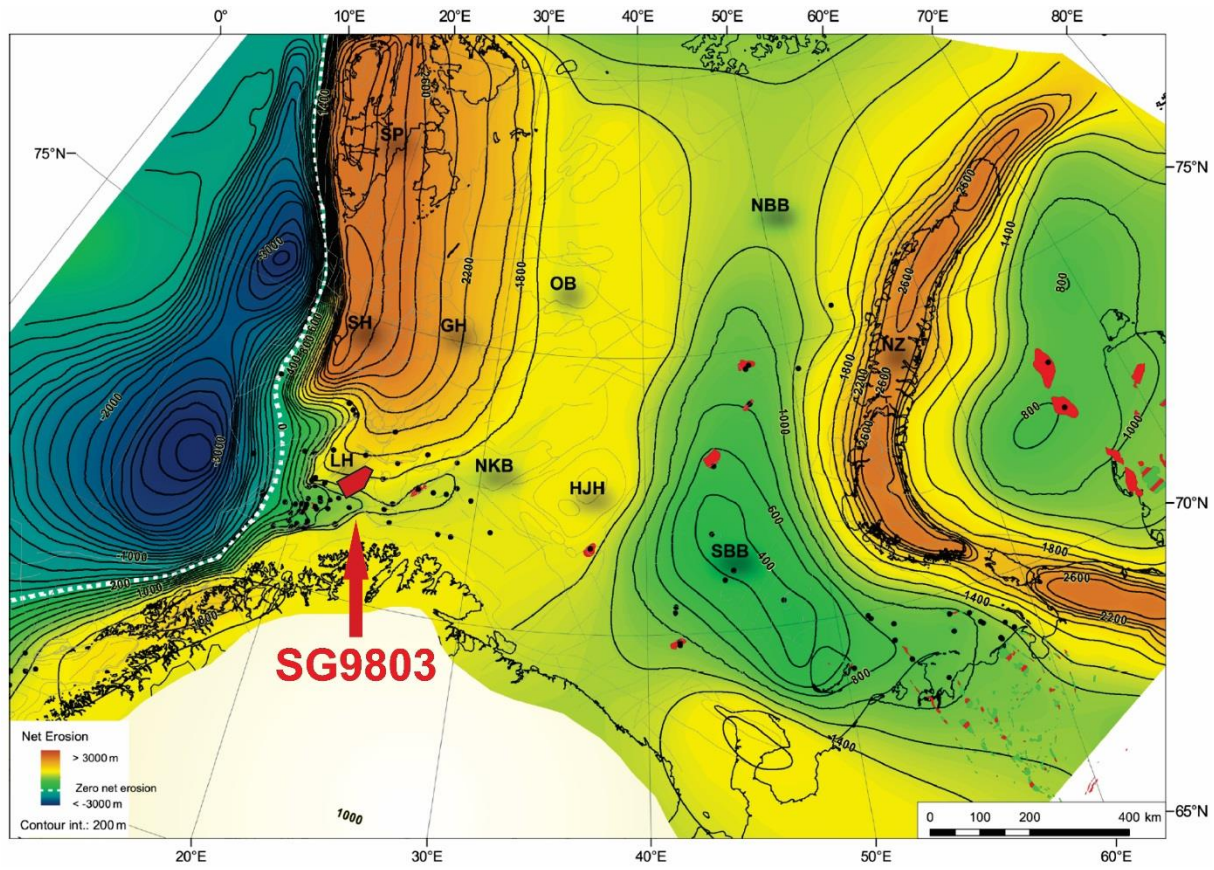

Figure 2-3: A regional map of the Greater Barents Sea illustrating the net erosion. Over the entire Barents Sea region net erosion ranges from 0 to > 3000 m. Location of survey SG9803 is marked as red (not to scale). Modified from Henriksen et al. (2011 b).

3 Data & methods

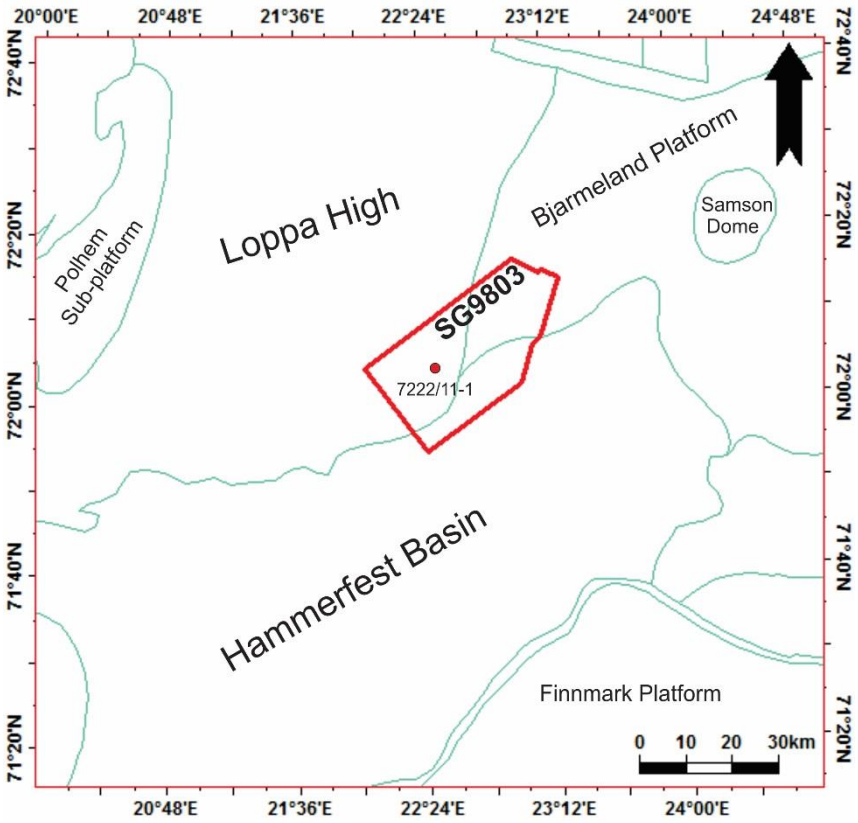

Figure 3 -1: Overview of the datasets used. Seismic dataset SG9803 as indicated. Wells 7222/11-1 can be seen as red dots.

3.1 Datasets

This study is based on the 3D seismic dataset SG9803 located in the southwestern Barents Sea, along with the exploration well 7222/11-1 to correlate seismically stratigraphic units.

3.1.1 Seismic data

The seismic 3D dataset SG9803 was collected by Saga Petroleum in 1998 and provided the support for well 7222/11-1 (NPD, 2016). See table 3.1 for more detailed info.

The convention adopted for the seismic polarity, is that of SEG (Society of Exploration Geophysicists) standard. In the SEG standard polarity, convention is based on a negative water-bottom reflection coefficient, which corresponds to a positive polarity. Thus, the zero-phase wavelet will be symmetrical

with respect to zero time and will peak at zero time. For SEG reverse polarity, it is flip-sided. The minimum phase wavelet has a short time duration and a concentration at the start of the wavelet, thus it begin with a “down kick” and is zero before zero time (Yilmaz, 2001).

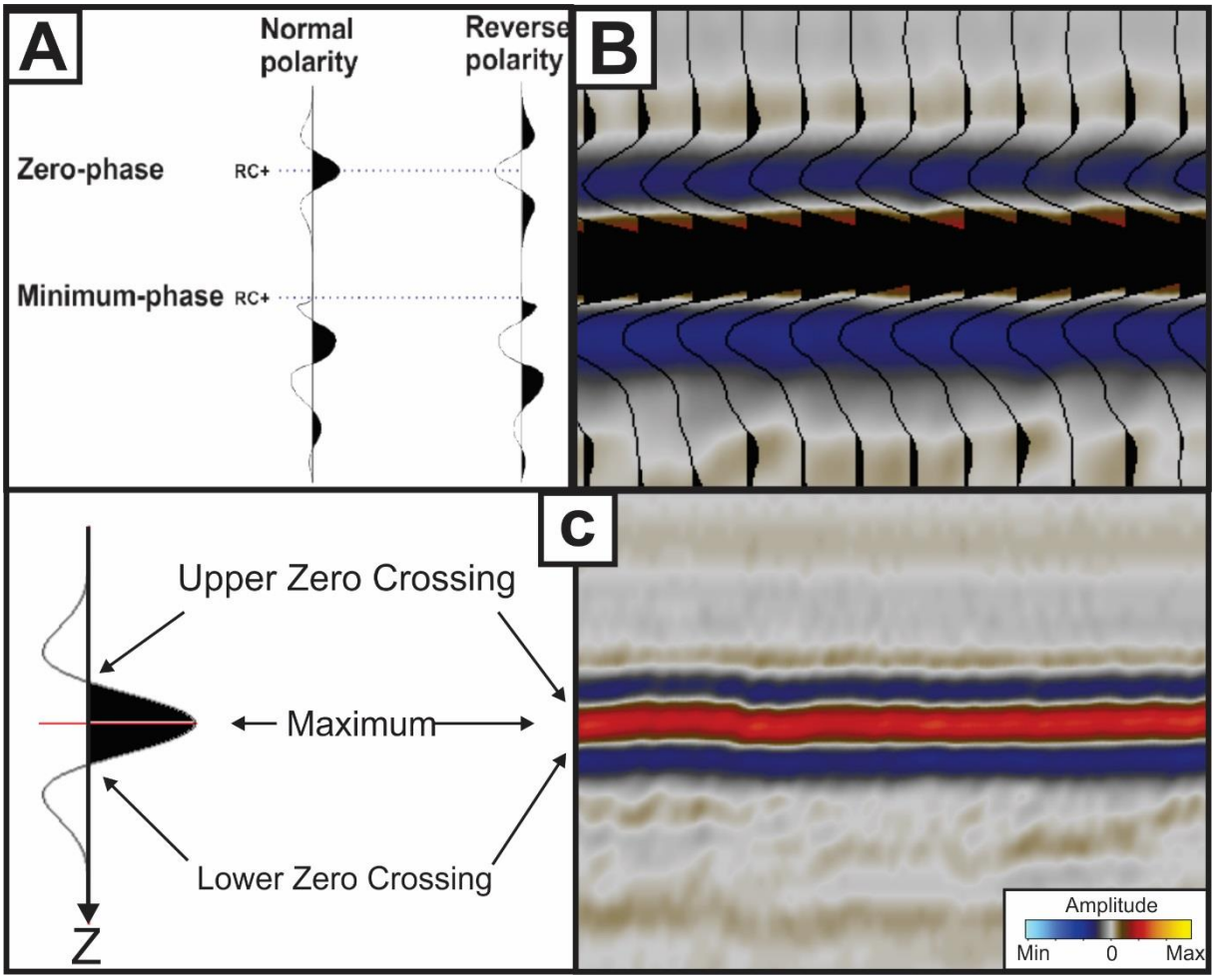

*Figure 3-2: **A:** Overview of SEG polarity convention. Normal zero-phase is used for this study (Sheriff, 2006). **B:** A zero-phase signal with positive polarity from the seabed reflection in SG09803. Positive amplitude is given in red/yellow, while negative amplitude is given in blue. **C:** Explanation of terminology used on the seabed reflector seen in B.*

Table 3-1: Overview of seismic information used in SG9803. Location of SG9803 can be seen in Figure 3-1.

Polarity	Phase	Dominating frequency (Hz)	Area (km^2)	Inlines	Crosslines	Inline orientation
Normal	Zero-phase	40	850	1824	3643	NW - SE

3.1.2 Well data

Well 7222/11-1 (Fig 3.1) was drilled in 2008 with the Polar Pioneer platform, with its primary objective being to prove possible hydrocarbon accumulations in middle and upper Triassic reservoir rocks. It did contain both oil and gas, in which exploitable gas accumulation is estimated to be between 2 – 14 billion Sm^3. However, due to poor reservoir qualities, in addition to complicated formation structures, it is temporary plugged and abandoned (NPD, 2008). The well data is used to determine age of seismic units and reflectors. See table 3.2 for more detailed info.

Table 3-2: Overview of information of lithostratigraphic units found in well 7222/11-1. Location of 7222/11-1 can be seen in Figure 3-1.

Interval	Top depth TWT (ms)	Top depth TVD (m)
Water column	-	-
Nordland GP	531	379
Kapp Toscana GP	591	451
Fruholmen FM	703	589
Snadd FM	740	636
Kobbe FM	1620	2007

3.2 Seismic interpretation and indications of fluids

Seismic mapping is a geophysical technique where the aim is to map geological structures from reflection of seismic waves. The waves are created from a seismic energy source and by examining the travel time of these waves caused by rock interfaces, known as reflectors, we can "map" the subsurface layers and structures of the earth.

Their own acoustic impedance, Z, defines the subsurface layers, which is defined as:

$$Z = \rho \cdot v \qquad \text{Eq 3.1}$$

Where ρ = density, and v = velocity.

The reflection strength at a boundary is governed by a reflection coefficient and can be quantified between -1 < R < 1 with the following equation

$$R = \frac{(Z_2 - Z_1)}{(Z_2 + Z_1)} = \frac{(\rho_2 v_2 - \rho_1 v_1)}{(\rho_2 v_2 + \rho_1 v_1)} \quad \text{Eq 3.2}$$

Where

R = the reflection coefficient

ρ_1 = density of medium 1, v_1 = velocity of medium 1

ρ_2 = density of medium 2, v_2 = velocity of medium 2

The physical nature of rocks determines if the reflection coefficient will be positive or negative, that is "softer" overlying "harder" rocks or vice versa. An obvious result of the reflection coefficient equation is that stronger amplitude yields stronger reflections. In most cases, the magnitude and reflection are determined by geological conditions, thus forming a connection between reflections and geology (Andreassen, 2009).

3.3 Seismic Resolution

Seismic resolution is the ability to differentiate how close reflectors can be, yet still be distinguished. There are two points of resolution – vertical and horizontal, both of which are controlled by signal bandwidth. Seismic velocities will generally increase with depths, as compression will take place and cause diminishing resolution due to decreasing frequencies (Yilmaz, 2001). In 3D seismic data you can see an object if it is larger than either the vertical or horizontal resolution (Rafaelsen, 2006).

The relationship between velocity, frequency and wavelength with increasing depth can be seen in (Figure 3.2). The dominant wavelength of seismic waves is given by:

$$\lambda = \frac{v}{f} \quad \text{Eq 3.3}$$

Where v is velocity and f is the dominant frequency.

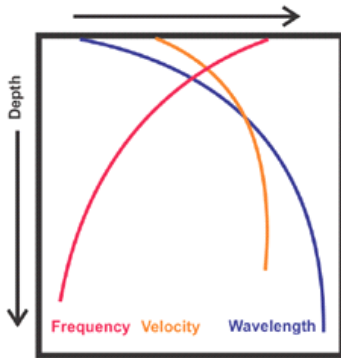

Figure 3.4 – The relationship between velocity, frequency and wavelength with increasing depths. Taken from (Brown 1999).

3.3.1 Vertical Resolution

The standard basis for vertical resolution is the dominant wavelength (Eq 3.3). To distinguish two reflections, one from the top and one from the bottom of a thin layer, there is a limit on how close they can be, yet still separable. This limit is governed by the layer thickness, and is the core issue of vertical resolution as wavelengths determines the resolution. The general acceptable threshold for vertical resolution as a limit of separability is a quarter of the dominant wavelength, and is the smallest separation of two wavelengths at a given time (Eq 3.4) (Yilmaz, 2001).

$$V_r = \frac{\lambda}{4} \qquad \text{Eq 3.4}$$

3.3.2 Horizontal Resolution

As sound wave fronts travels in three dimension spherically, the horizontal resolution is governed by the Fresnel zone and refers to how close two reflection points can be situated horizontally, yet be recognized as two separate points rather than one. Thus, to distinguish lateral elements on seismic data, the elements needs to exceed the Fresnel zone (Yilmaz, 2001).

The Fresnel zone is defined in Figure 3-5 A.

Hence, the radius of wave fronts may be approximated to:

$$r = \sqrt{\frac{z_0\lambda}{2}} = \frac{v}{2}\sqrt{\frac{t_0}{f}} \qquad \text{Eq 3.5}$$

In 3D seismic, the Fresnel zone is reduced to an eclipse perpendicular to a small circle with higher focus and resolution (Figure 3-5 B). The Horizontal resolution is thus given as:

$$H_r = \frac{\lambda}{4} = \frac{v}{4f} \qquad \text{Eq 3.6}$$

By using Eq 3.6 and a p-wave velocity of 1800 ms (average glacial sediment velocity), the horizontal resolution of SG9803 is calculated to 11.25 m.

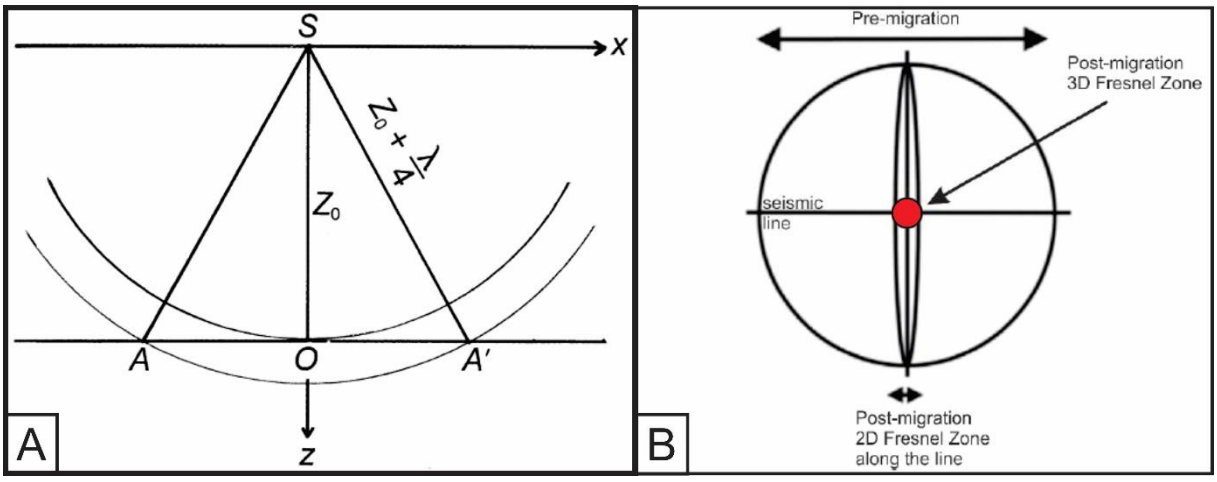

*Figure 3.5: **A** – The definition of the Freznel zone in terms of dominant frequency, f. Taken from (Yilmaz, 2001)..**B**: – The focusing effect of migration in two and three dimensions. The small red circle depicts the 3D migration. Modified from (Rafaelsen, 2006).*

3.4 Artefacts

Artefacts can take place in seismic data and interferers the data and/or may cause misinterpretation. The artefacts found in SG9803 are related to the acquisition of the data, which appears as parallel lines in the same directions as the gathering vessel at the surface, and as "faults" beneath them (Figure 3.6). These are called seismic acquisition marks, and avoided by altering the light settings, but can still be noticed.

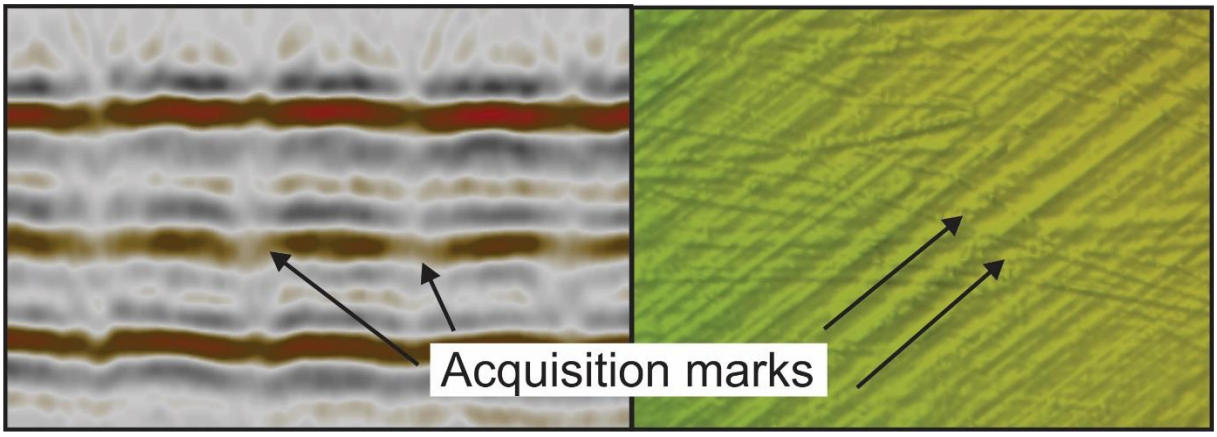

Figure 3.6: Seismic profile showing the occurrence of seismic acquisition marks. Sub-surface as horizontal lines to the left and parallel lines on the surface.

3.5 Software

3.5.1 Petrel

Petrel is the primary software used in this thesis. Petrel is a tool owned by Schlumberger and is an exploration and production software platform used by the petroleum industry. It allows the user to interpret seismic data, perform well correlation, calculate volumes, and produce maps and so forth. Depth of seismic data is given in two-way travel time (TWT).

RMS (root mean square) amplitude maps are used to map out amplitude anomalies in areas associated with fluid flow. The RMS attribute map calculates the sum of average amplitude values for a given window. These values are then squared in order to avoid negative values before the square root is used. This process causes enhancement of seismic amplitudes allowing easier identification of zones of interests, as the impedance contrast between sediments and morphological structures are heightened. Time thickness maps are used to map out the TWT between two surfaces, which is further used to illustrate the thickness and extent of seismic units.

3.5.2 CorelDraw

Figures used in this thesis are made through CorelDraw, a vector graphic editor.

4 Seismic stratigraphy

This chapter will focus on the description of the seismic reflectors and units interpreted within the 3D dataset SG9803. The three reflectors described in this study are the base canyon, the upper regional unconformity (URU), and the seafloor (the URU and seafloor coincides in the southwestern parts of the area). An overview of the reflectors is shown in (Figure 4-1). Depths are given in two way travel time (ms).

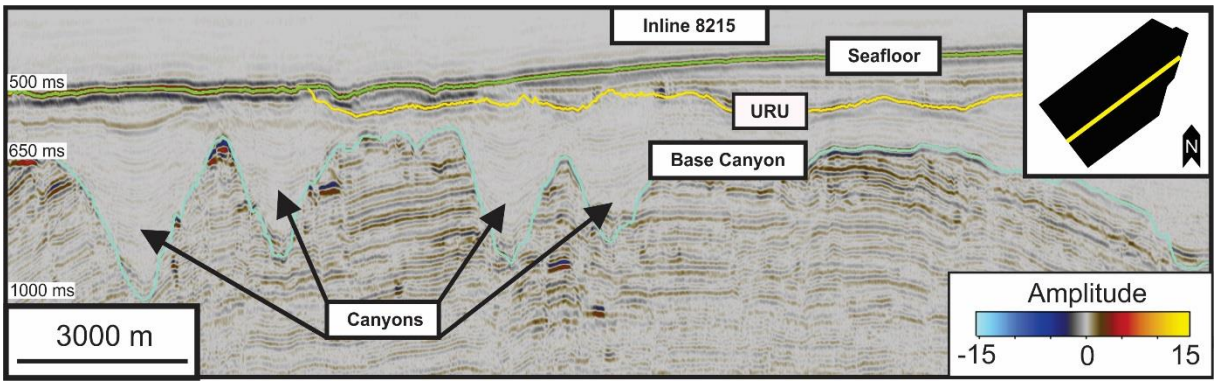

Figure 4-1: Inline 8215 illustrating the interpreted reflectors. The seafloor reflector is shown in green, the URU in yellow and the base canyon as teal. Notice that the URU is truncated by the seafloor reflector.

4.1 Main reflectors

4.1.1 The base canyon reflector

4.1.1.1 Description

The base canyon reflector (Figure 4-1) is situated between 553 to 1635 ms TWT. The base canyon reflector is discontinuous, and truncates the underlying Mesozoic strata (Figure 4-2). Hence, the base canyon is an angular unconformity (Figure 4-2 B).The reflector displays five V-shaped canyons in its middle parts (Figure 4-2 C), and a significant depression towards southeast (Figure 4-2B). The canyons displays a decreasing trend in size from southwest towards northeast.

Canyon #1 is situated on the western side and the white dotted line marks its southeastern termination (#1 at Figure 4-2 C). Canyon #1 is up to 3500 m at its widest. The canyon reaches depths of 1200 ms TWT and with a length of up to 18000 m along its longest path. The canyon has a meandering shape, and divides into two major paths.

Canyon #2 (Figure 4-2 C) has a width of up to 3000 m at the crests with alternating continuous to discontinuous reflections at its interface (Figure 4-2 A, C & Figure 4-10). The canyon is mostly situated on depths of about 700 to 800 ms TWT, although depths down to 900 ms TWT exists. Canyon #2 also show meandering character, but to a lesser extent. The bottom base length of canyon #2 is about 15000 m, and it divides and branches out towards northwest.

Canyon #3 and #4 (Figure 4-2 C) displays similar properties and has an upper width of up to 2000 m between the shoulders, but differs in horizontal orientation. They are situated on depths of about 900 ms TWT. Meandering is far less prominent in these canyons, and there are little to no sign of branching at their termination points.

Canyon #2 (Figure 4-2 C) is the smallest one, and it is situated in an area where the data quality is poor as the reflector is discontinuous with low to medium amplitude. The width is up to 800 m. The length of the canyon is measured to around 3000 m, but it may continue further northwards. It is situated slightly above the others on a depth of about 800 ms TWT.

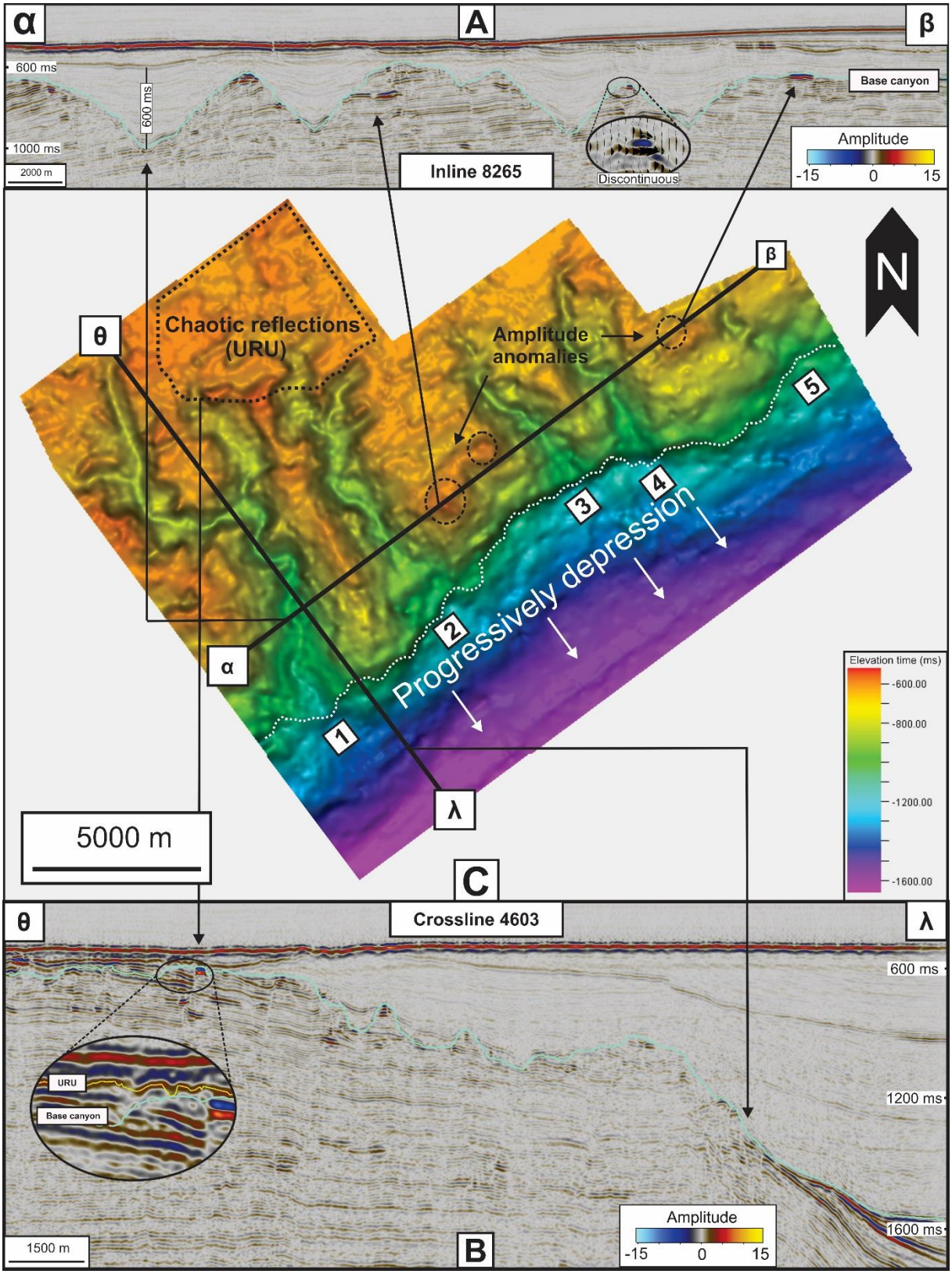

*Figure 4-2: **A**: Inline 8265 illustrating the base canyon reflector in teal. **B**: Crossline 4603 illustrating the base canyon reflector in teal. **C**: Surface of the base canyon reflector. The black seismic line refers to the profiles shown in (A) and (B). Canyon features are indexed as 1 to 5. See figure 5-1 for reflector overview. Vertical exaggeration set to 10x.*

4.1.1.2 Interpretation

The base canyon reflector (Figure 4-2) is a result of erosional processes taking place under regional uplift of the Loppa High. According to (Gabrielsen et al., 1990), the Loppa High was an island during most of the Cretaceous, being eroded along its margins by deep canyons cutting into the Triassic sequences supplying submarine fans to the surrounding basins (Faleide et al., 1993). Cretaceous sequences appear as units that onlap and infill these erosional valleys.

The base canyon reflector (Figure 4-2) is a result of erosional processes taking place under regional uplift of the Loppa High. According to Gabrielsen et al. (1990), the Loppa high was uplifted during Late Jurassic to Early Cretaceous time, and continued as an island during most of the Cretaceous. The uplift lead to erosion along the margins creating deep erosional valleys or canyons cutting into Triassic sequences, and hence, forming submarine fans in the surrounding basins (Faleide et al. 1993).

As the reflector dip from northwest to southeast, the sediment thickness and depositional environments differs and hence, the reflector shows varying reflection characteristics along its path due to erosion of different lithology (Fig 5-9 B). In high areas close to the URU reflector (Figure 4-2 B), the reflector is discontinuous with low to medium amplitude, which may be credited to erosional deglaciation processes leaving only resistance surfaces and/or combined with underlying fluid migration.

4.1.2 The URU: upper regional unconformity

4.1.2.1 Description

In general, the URU is quite continuous. The URU is truncated by the seafloor in southwestern areas. It spans from 474 to 652 ms in TWT. Its amplitude is mostly strong. The seismic tracking of the URU in SG9803 is based on the work of a previous master thesis (Midtbø, 2000). The URU will further be described in two sub-divisions based on the topography (Figure 4-3 B).

Area I (Figure 4-3 & Figure 4-4) is rather flat and ranges from 475 to 550 ms TWT, with the shallowest part in the northeast, dipping towards the southwest. A prominent feature in area I is the northwest-orientated depression in the southwestern part, which extends up to 4400 m in width. The area is also

covered with small circular depressions with depths up to 25 ms and widths up to 500 m (Figure 4-4 A & C). Linear marks with a northeastern direction is situated along the surface.

Area II (Figure 4-5) is about 550 km^2, and ranges from 510 to 650 ms TWT in depth and shows a trend of alternating amplitude strengths, with some discontinuity. The middle parts shows a large depression, which is up to 600 ms deep and 3000 m long (Figure 4-3 B & D). The depression is also adjacent to circular depressions (B & D) which is the deepest parts of the URU reflector, consisting of depths up to 650 ms and diameters up to 2000 m. Discontinuous areas are present in the southwestern areas (Figure 4-3 A & D). Two linear depressions are present in the northeastern areas (Figure 4-5 A & D) with lengths of about 13000 m and depths up to 15 ms.

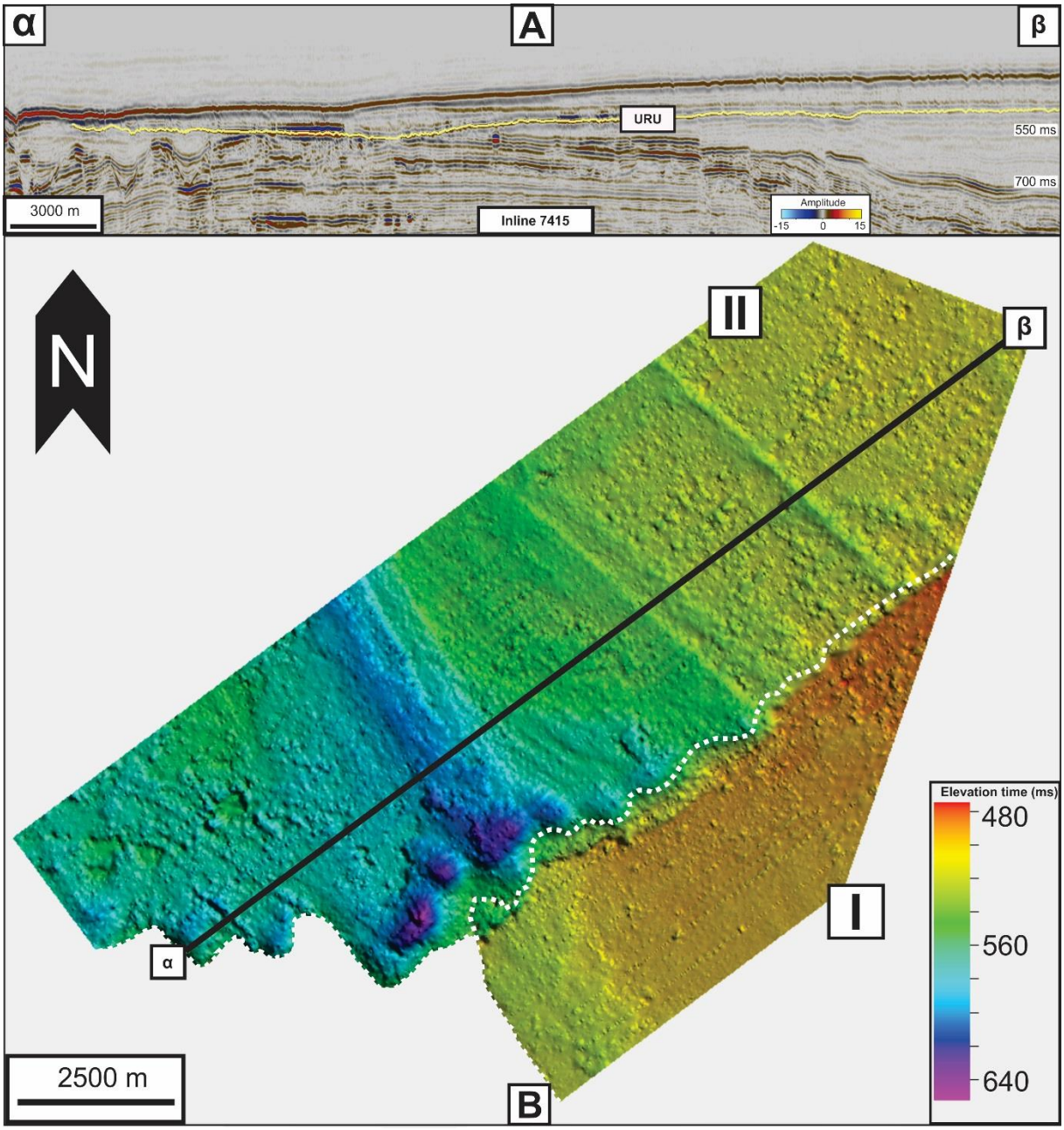

*Figure 4-3: **A**: Inline 7415 illustrating the extent of the URU reflector. **B**: Surface of the URU reflector. The black line refers to seismic inline 7415. Dotted white line illustrates the topographical sub-areas for further interpretation. Vertical exaggeration set to 10x.*

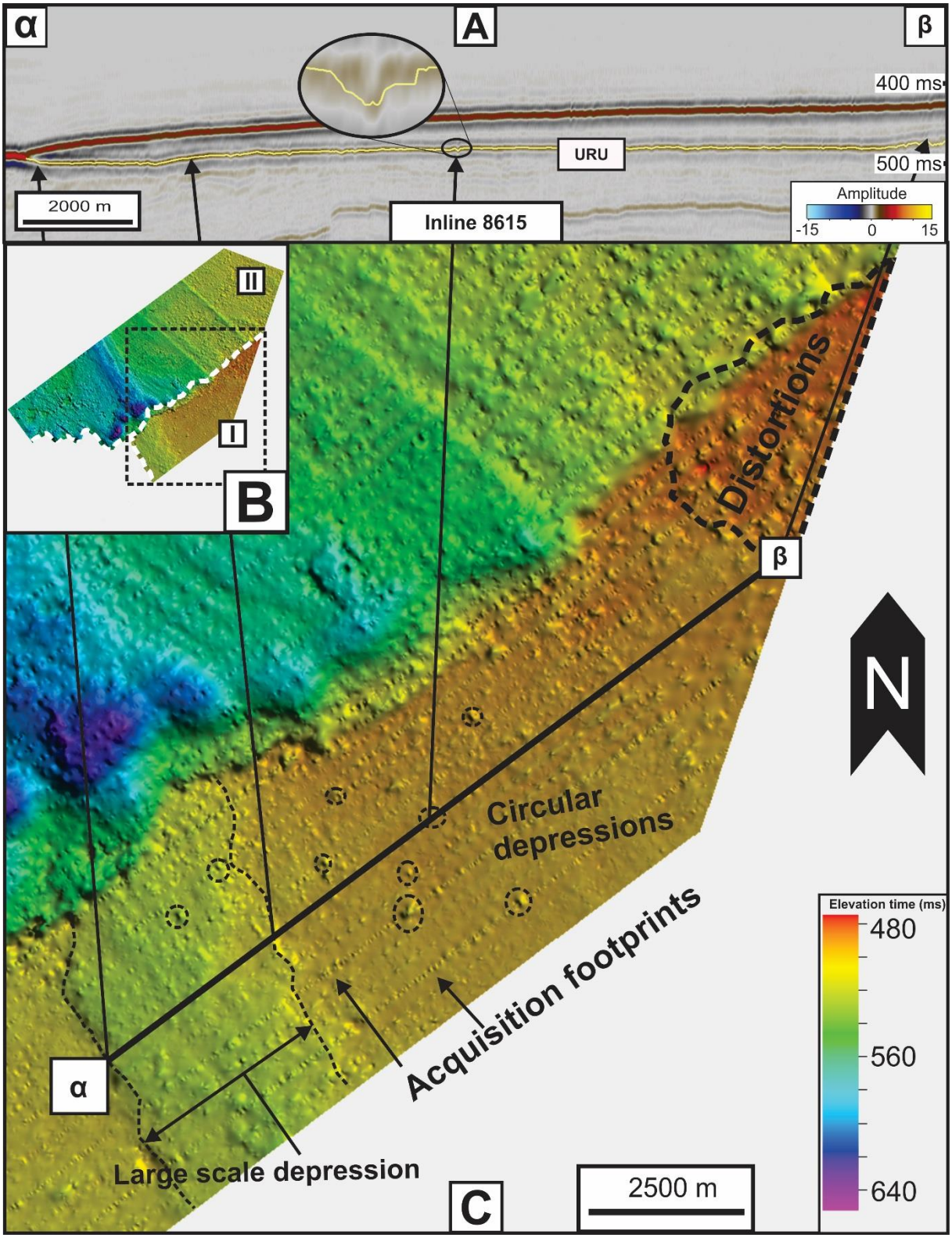

*Figure 4-4: **A**: Inline 8615 illustrating the URU reflector. **B**: Sub-divisions used of the URU reflector surface. C: Enlarged map of URU surface area I. The black seismic line refers to the seismic profile shown in (A). Vertical exaggeration set to 5x.*

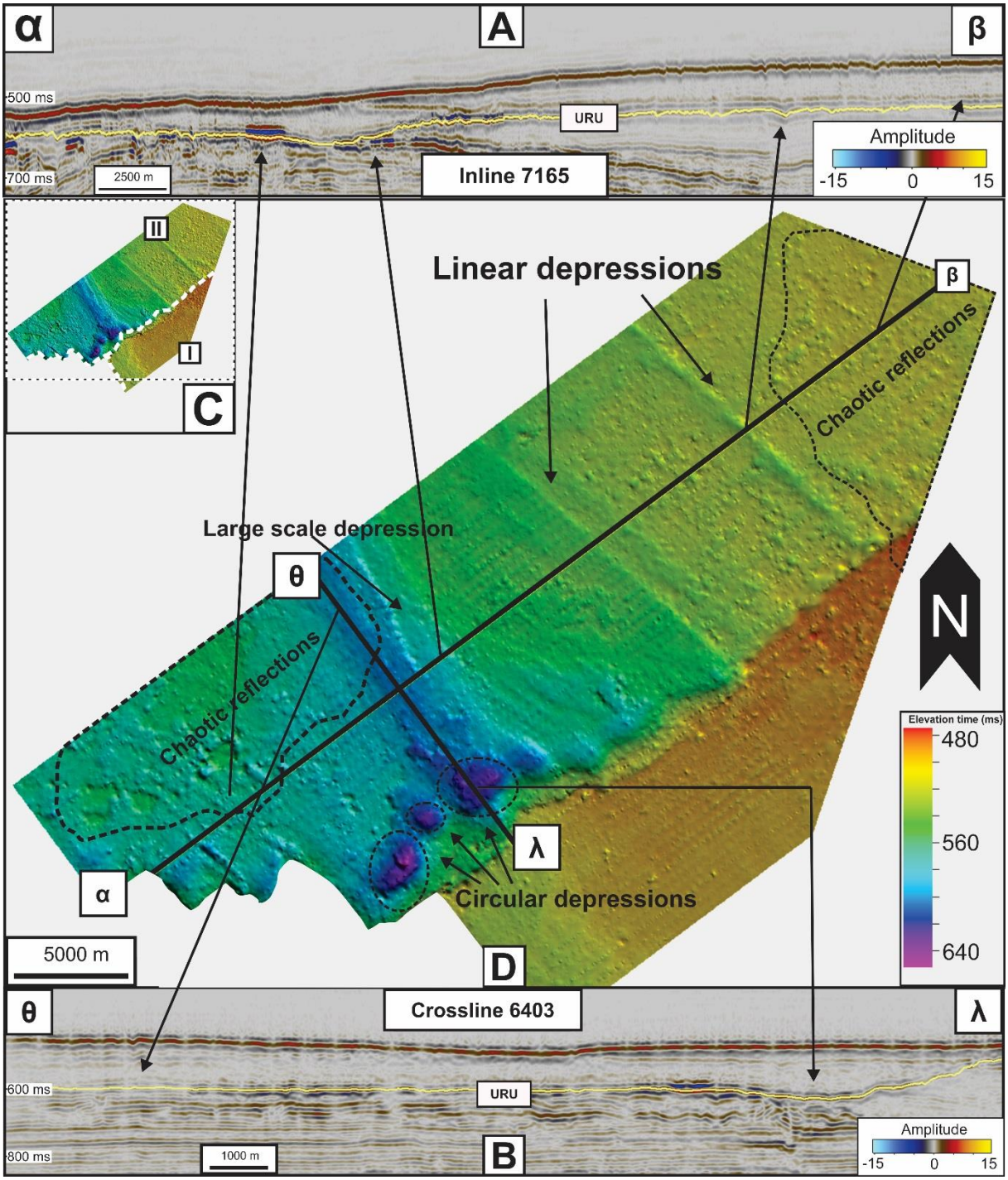

*Figure 4-5: **A**: Inline 7165 illustrating the URU reflector. **B**: Crossline 6403 illustrating the URU reflector. **C**: Sub-divisions of the URU reflector surface. **D**: Enlarged map of URU surface area II. The black seismic lines refers to the profiles shown in (A) and (B). Vertical exaggeration set to 5x.*

4.1.2.2 Interpretation

The URU (Figure 4-3) is a regional erosion surface found in the Barents Sea, and defines the base of the glacigenic sediments on the shelf (Vorren & Kristoffersen, 1986).

Area I (Fig 5-7) is a rather homogenous surface, in terms of depths and erosional patterns, which is likely caused by a rock that exhibits resistance towards erosion. However, there is one prominent feature - a large-scale depression, spanning some 4400 m at its widest. This depression is likely a paleo-trough of ice stream origins, which seems to continue in Area II. The circular depressions of area I is hard to interpret, as the underlying seismic resolution is poor (Figure 4-4) and artefacts were difficult to remove. The circular depressions could be paleo pockmarks and/or seismic acquisition artefacts.

Amplitude anomalies are seen beneath the surface of area II (Figure 4-5 B), which is likely caused by underlying fluids. This explains the circular depressions (Figure 4-5 B & Figure 4-5 D), and is likely explained through underlying fluids (I.e. pockmarks), which is likely linked with accumulation of gas in sediments in the region. These depressions also correlate with both depressions further explained on the seafloor.

4.1.3 The seafloor reflector

4.1.3.1 Description

The reflection has a continuous high amplitude. The depths to the seafloor ranges from 360 ms to 580 ms TWT, and has a southwesterly dip. The seafloor is divided in three sub-areas (I, II& III)(Figure 4-6).

In the northeast (Area I in Figure 4-6 C) the seafloor is dominated by furrows. These furrows ranges from depths of 1-10 ms TWT and widths of 50 m to 150 m and their numbers decline from northeast towards southwest as the water depths increase. The deepest furrows are found on depths of 570 ms TWT. A majority of the furrows exhibits an east-west orientation. In the western part of area I there is a slope that ranges from 0.5 degrees in the northern parts and 2.5 degrees further south. The southern parts of the area is very smooth and horizontal, although it exhibits a small southwesterly incline.

A prominent slope separates area I and II in the eastern part of the study area (Figure 4-7 A & C). Some small circular depressions occur, with widths up to 100 m. Furrows are also present here, but they are

much shorter in extent. The transition towards south is dominated by the topographical changes of area III (Figure 4-7 C).

Area III (Figure 4-8) covers the southern and deepest area of the survey, opposed to area I & II the topographic characteristics is different, which is caused by truncation of the URU reflector (Figure 4-8 A). The area is overall very rugged. The most prominent feature found in this area is a southwestern orientated meandering depression located in the central part of area III. This depression is about 50 ms deep and up to 650 m wide (Figure 4-8 A & C). The seabed is rather flat and smooth north of this feature, with some minor furrows of random directions, with a circular depression towards northwest. The southern parts of area III also exhibits depressions and minor furrows. The depressions of Area III correlates with subsurface high-amplitude areas (explained in the seismic unit section).

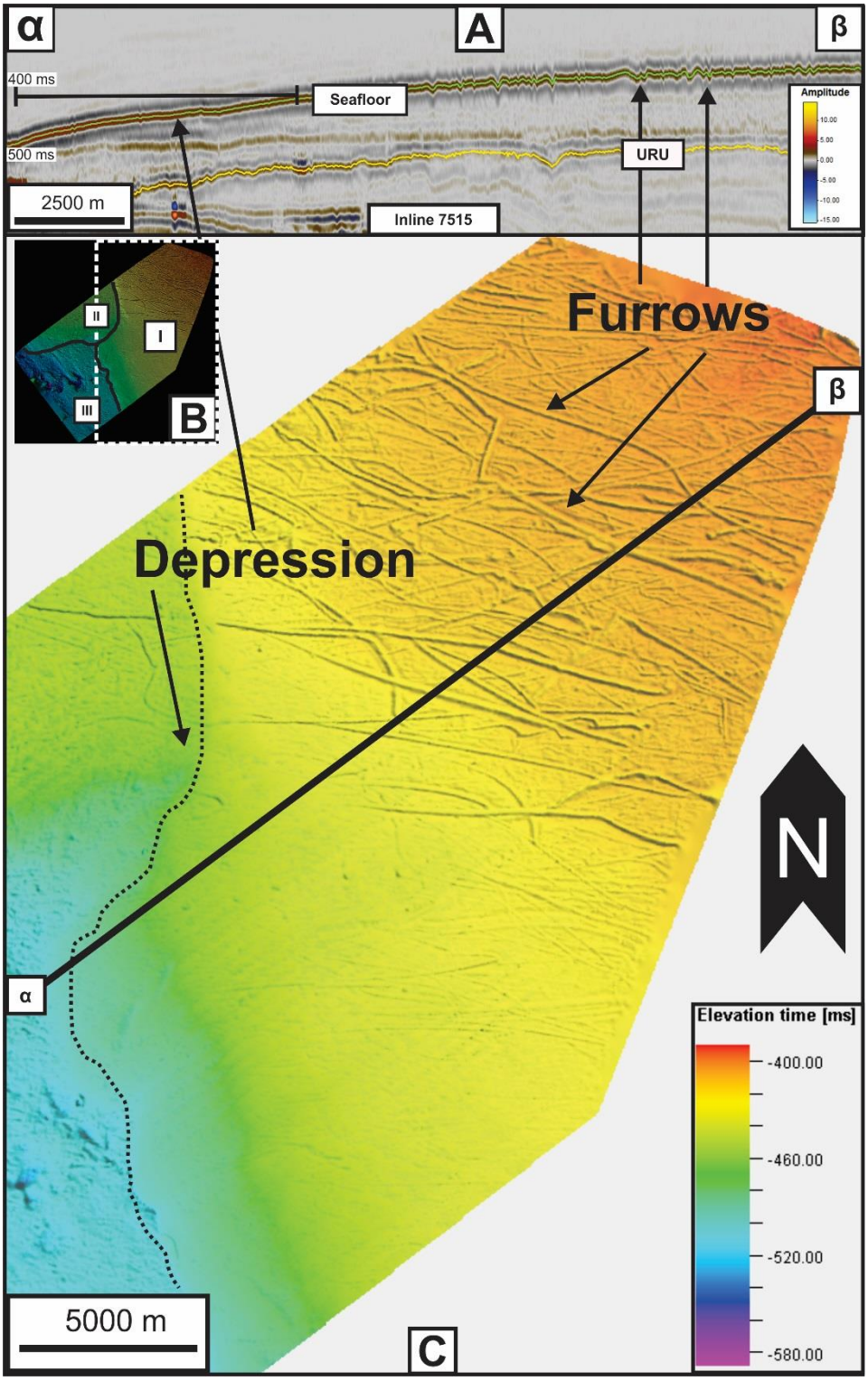

*Figure 4-6: **A**: Inline 7515 illustrating the seafloor reflector in green. **B**: Sub-divisions of the seafloor areas. **C**: Enlarged map of seafloor area I. The black seismic line refers to the profile shown in (A). Vertical exaggeration set to 10x.*

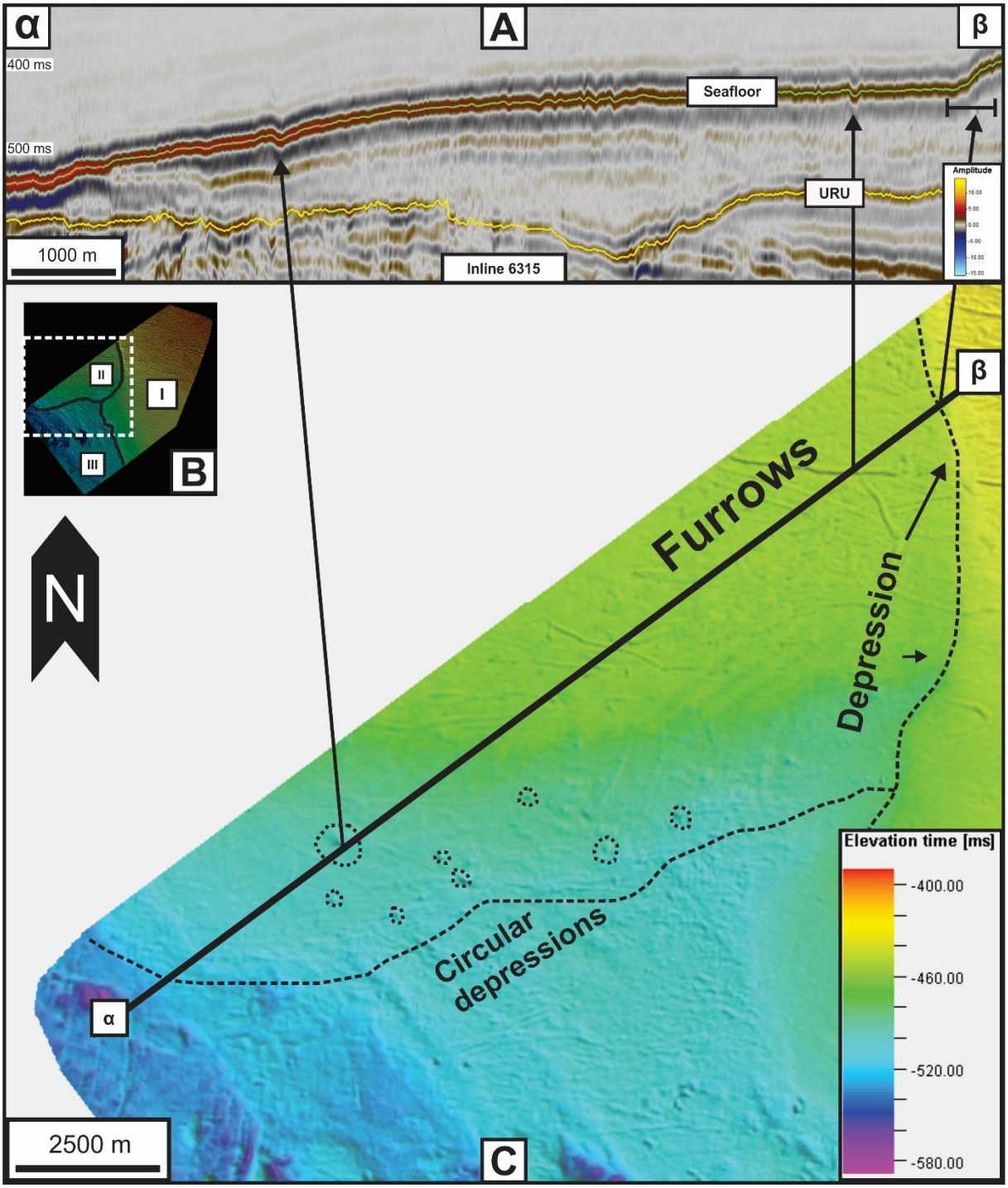

*Figure 4-7: **A**: Inline 6315 illustrating the seafloor reflector in green. **B**: Sub divisions within the seafloor area. **C**: Enlarged map of seafloor area II. The black seismic line refers to inline 6315 shown in (A). Vertical exaggeration set to 10x.*

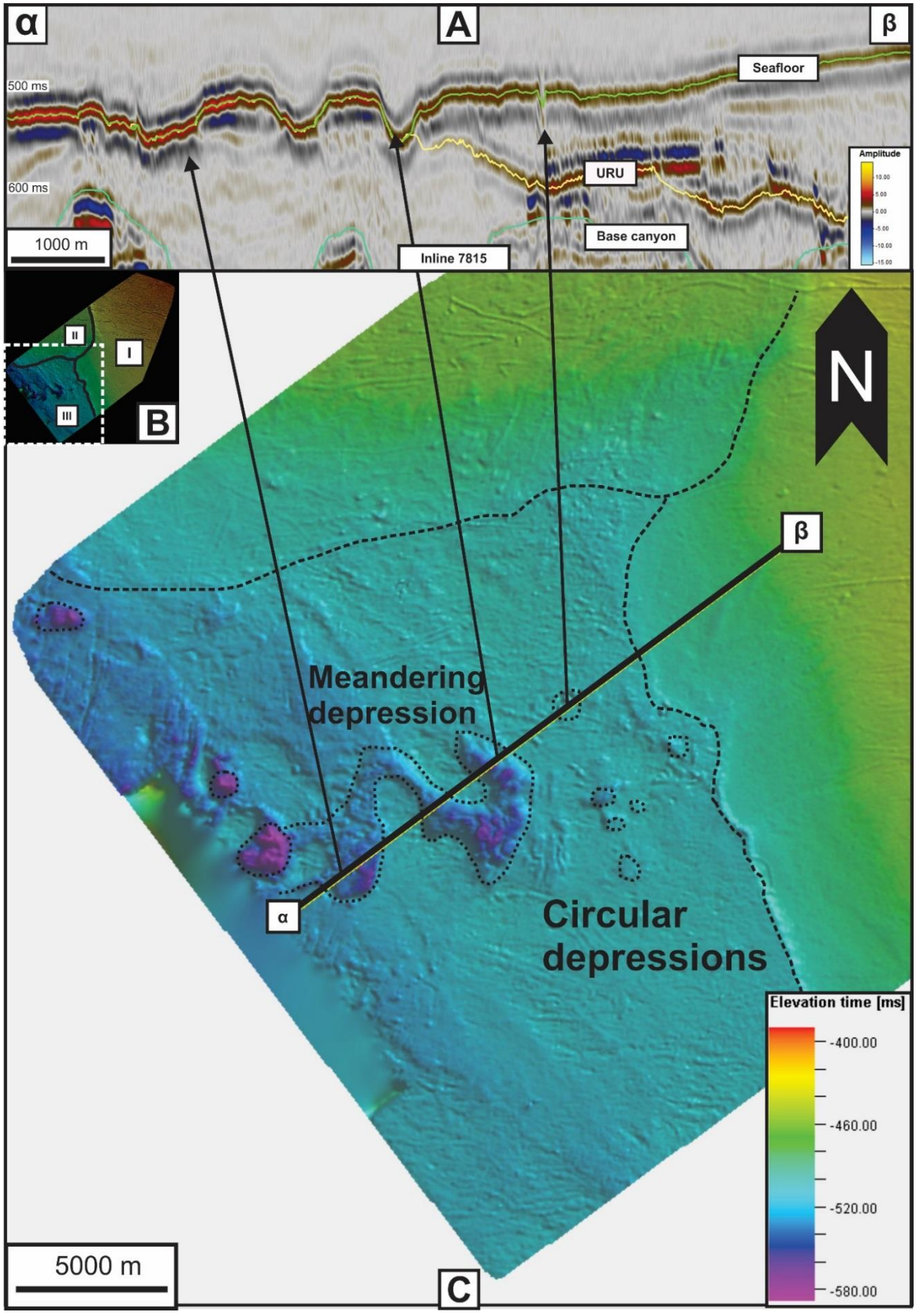

*Figure 4-8: **A**: Inline 7815 illustrating the reflectors interpreted. The seafloor reflector is shown in green and the URU reflector in yellow. Notice that the URU reflector is truncated by the seafloor reflector. **B**: Sub-divisions of the seafloor areas. **C**: Enlarged contour map of seafloor area III. The black seismic line refers to the profile shown in (A). Vertical exaggeration set to 10x.*

4.1.3.2 Interpretation

Area I is rather planar, with a slight incline towards east, and prominent furrow features (Figure 4-6), which are likely caused by iceberg plough marks, a common seafloor feature found in the latitudes of SW Barents Sea (Andreassen et al., 2008) . The plough marks does generally show an east western orientation. The width and depth of the plough marks, up to 150 m wide and 10 ms deep, reveals that the icebergs must have been of considerable size. All though the majority of plough marks show an east western orientation, there is a lesser amount of intersecting plough marks, yet they are of smaller nature - a feature that could be caused by temporary changing sea ice dynamics. The depressions around area I are situated within the Ingøydjupet Trough, a trough that was eroded by fast-flowing ice streams during the last glacial maximum (Winsborrow et al., 2010).

Area II does also display furrows which is likely caused by plough marks, yet they are smaller than those described in northern area I. Area II is situated on a depth of about 500 ms (Figure 4-7 C), a similar depth of that on southern area I, hence the icebergs need to reach deeper in order to gouge the seabed. Sediments accumulated in area II may have been caused by drifting from area I, as it is situated below and in the same direction as the plough marks.

Accumulation of hydrocarbon gas in sediments is known to take place in this region. This is caused as glaciations remove thick layers of seabed sediments, which triggers opening of pre-existing faults and creation of new ones, facilitating fluid migration and eventually escape from the sub-surface (Chand et al., 2012)

4.2 Seismic units

4.2.1 S0

4.2.1.1 Description

Unit S0 (Figure 4-9) is situated beneath the base canyon reflector. It and is about 400 ms at its thickest. Its thickness is governed by the lateral extent of the base canyon reflector (Figure 4-2). The internal reflection configuration varies between parallel and subparallel (Figure 4-9).

The internal reflection amplitudes are high and internal reflectors are rather continuous, but distortions appear around high amplitude areas (Figure 4-9).

Several high-amplitude anomalies are found along the ridges adjacent to the canyons (Figure 4-10 B). The density of amplitude anomalies are decreasing from west to south, and the strongest ones are located southwest of canyon #1 (Figure 4-10), and follow the ridges laterally as well (from southeast to northwest).

Acoustic masking and dim zones are observed beneath bright spots (Figure 4-9 & Figure 4-10) throughout the unit, and these extend through several internal stratigraphic units. These are especially prominent in proximity to faulting.

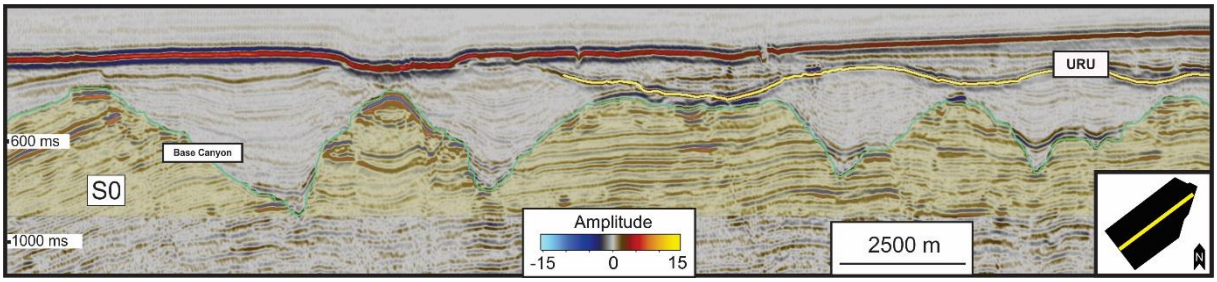

Figure 4-9: Inline 8065 illustrating the extent of S0 (shaded yellow) beneath the base canyon reflector (teal).

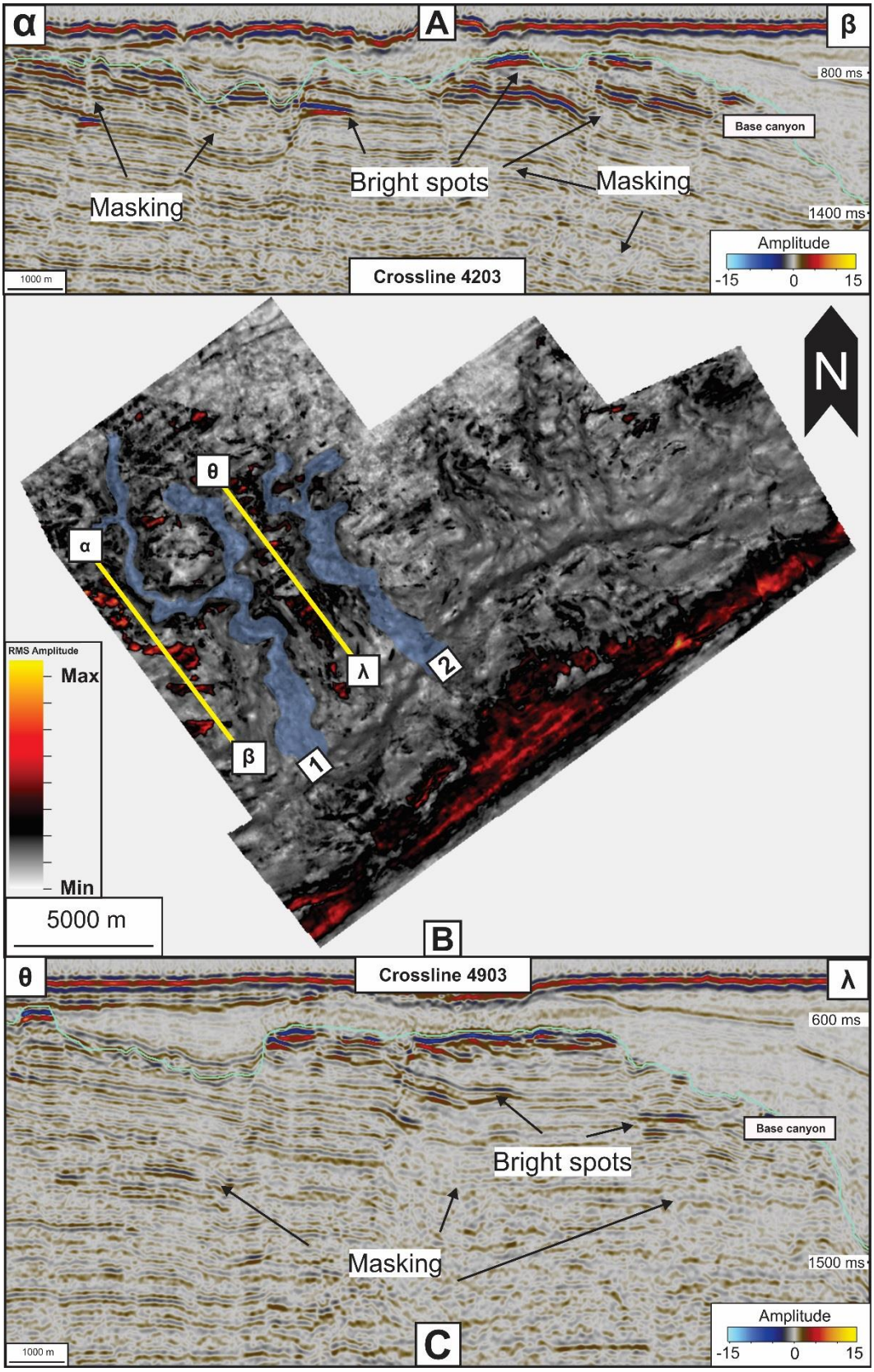

*Figure 4-10: **A**: Crossline 4203 along the seismic anomalies west of canyon #1. **B**: Crossline 4903 along the anomalies of the ridges between canyon #1 and #2. **C**: RMS amplitude map of seismic unit S0. The RMS search window is set to 25 below the base canyon surface. Yellow lines refers to the profiles shown in (A) and (B). Canyon #1 and #2 are shown as shaded blue.*

4.2.1.2 Interpretation

The parallel to wavy reflection characteristic is associated with uniform sedimentation conditions for the sequence on top of a subsiding substratum. Parallel geometry occurs in shallow waters, reflecting coastal plain or shallow marine depositional environments (Veeken, 2007). Earlier studies have shown that this unit is characterized by fluvial to shallow marine sedimentary environments. (Smelror et al., 2009; Henriksen et al., 2011 b). The upper termination limit of unit S0 is a result of later erosion, which subsequently formed the canyons.

Internal fluid migration is clearly visible within S0, as features such as dim zones and chimney structures (seen as distorted seismic) and local bright spots are present (Figure 4-10). The bright spots suggests accumulation of gas. Gas chimneys are associated with irregular distribution of low-velocity gas-charged zone, formed due to an upward migration of gas/fluids (Vadakkepuliyambatta et al., 2013).

4.2.2 S1

4.2.2.1 Description

Seismic unit S1 (Figure 4-11 & Figure 4-13 A) is situated between the base canyon and the URU (Figure 4-1), and is up to 1000 ms thick to its eastern/southeastern directions and gradually thins and pinch out towards west and northwest. The upper termination of S1 is truncated by the URU. The thickness is up to 500 ms within the canyons (Figure 4-13 A), which show signs of subparallel infill. Towards southeast, S1 shows tangential oblique features (Figure 4-11 B).

Unit S1 consists of rather discontinuous reflections internally (Figure 4-11 A). Disruptions also occurs. Internal amplitudes is generally weak, with some exceptions of medium amplitude reflections, such as those shown in the middle parts of Figure 4-11 B. Areas close to the canyon ridges of unit S1 (Figure 4-11 A) are characterized by a transparent reflection configuration and irregular reflections. High-amplitude areas in S1 are very few, but some are located in the western part of the survey (Figure 4-12).

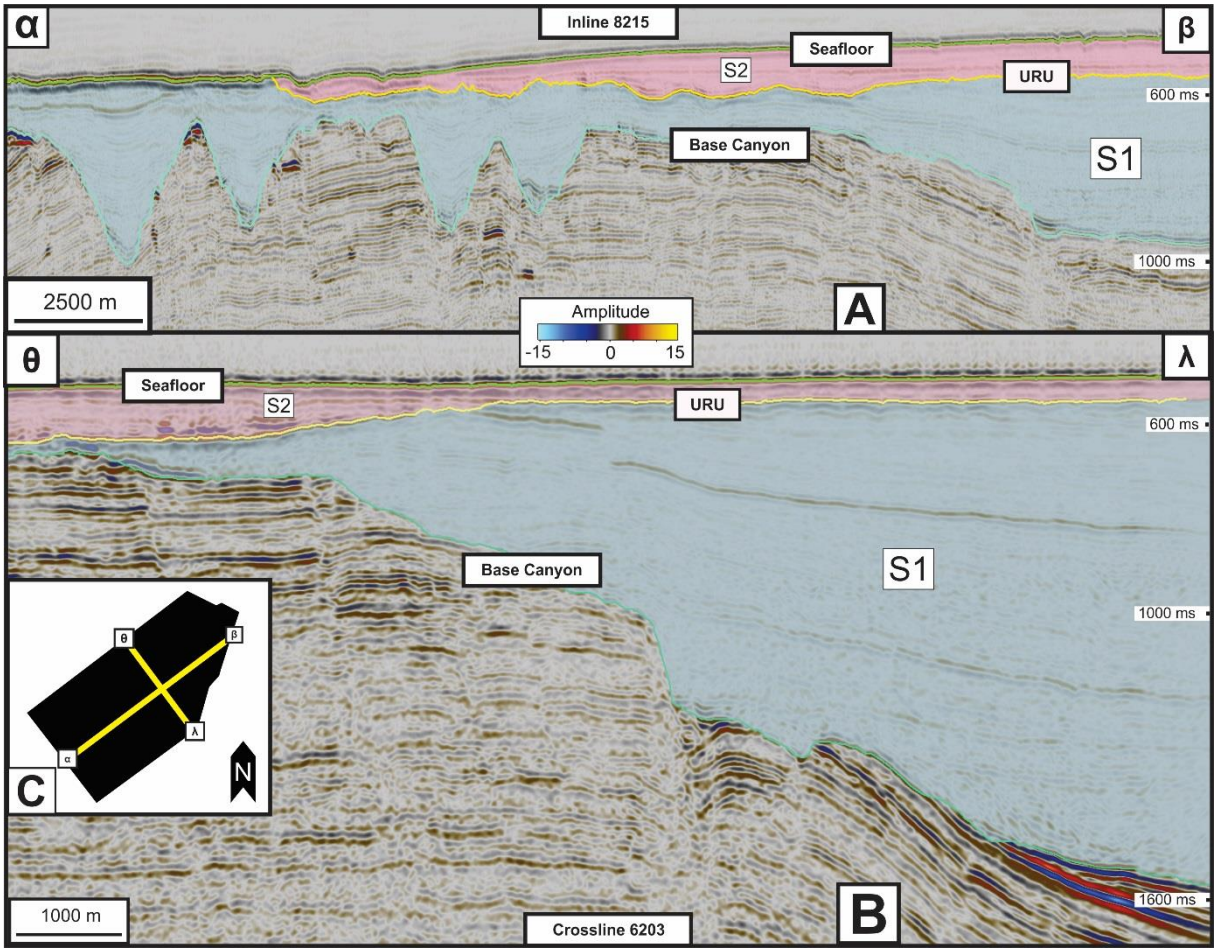

Figure 4-11: ***A:*** *Inline 8215 illustrating the reflectors used to define the unit boundaries. Seismic unit S1 is represented by the blue shade. Seismic unit S2 is represented by the red shade.* ***B****: Crossline 6203 illustrating the above seismic units* ***C:*** *Overview of the seismic lines used (in yellow).*

4.2.2.2 Interpretation

Both internal amplitudes and continuities of reflections of S1 (Figure 4-11) is poor, but they generally show a parallel to subparallel configuration, especially in lower parts of the canyons. Lower parallel to sub-parallel configuration is associated with the marine and shallow marine sedimentary environment, as the canyons were filled. Discontinuity in upper parts of S1 (Figure 4-11 A) is likely caused by different depositional environments and unconsolidated sedimentation and fluids trapped within sediments. The transparent reflections in areas close to the canyon ridges of unit S1 (Figure 4-11 A) are likely a result of fluid migration related to the canyon ridges of S0.

The thick south-southeastern section of S1 (Figure 4-11 B & Figure 4-13 A) is situated in the Hammerfest Basin. The seismic shows a direction of downward coastal onlap along the Loppa High slope, and sediments have likely eroded from Jurassic strata and deposited in the form of basin floor fans or turbidity lobes during the Cretaceous.

The high amplitude areas within S1 (Figure 4-12) is likely caused by the URU in this area, which acts as a less permeable barrier between the seafloor and S1, causing accumulation of fluids. Fluid migration within S1 correlates and is likely the cause of depressions seen in the seafloor, such as pockmarks and the crater structure (Figure 4-8 C). This is explained as high amplitude areas within S1 is close to non-existent, which suggests that fluids reaches the seafloor (i.e. no accumulation) and subsequently causing the depressions seen in the seafloor (Figure 4-7). Fluids also seems to migrate some parts upwards to S2 (later descripted in S2 section).

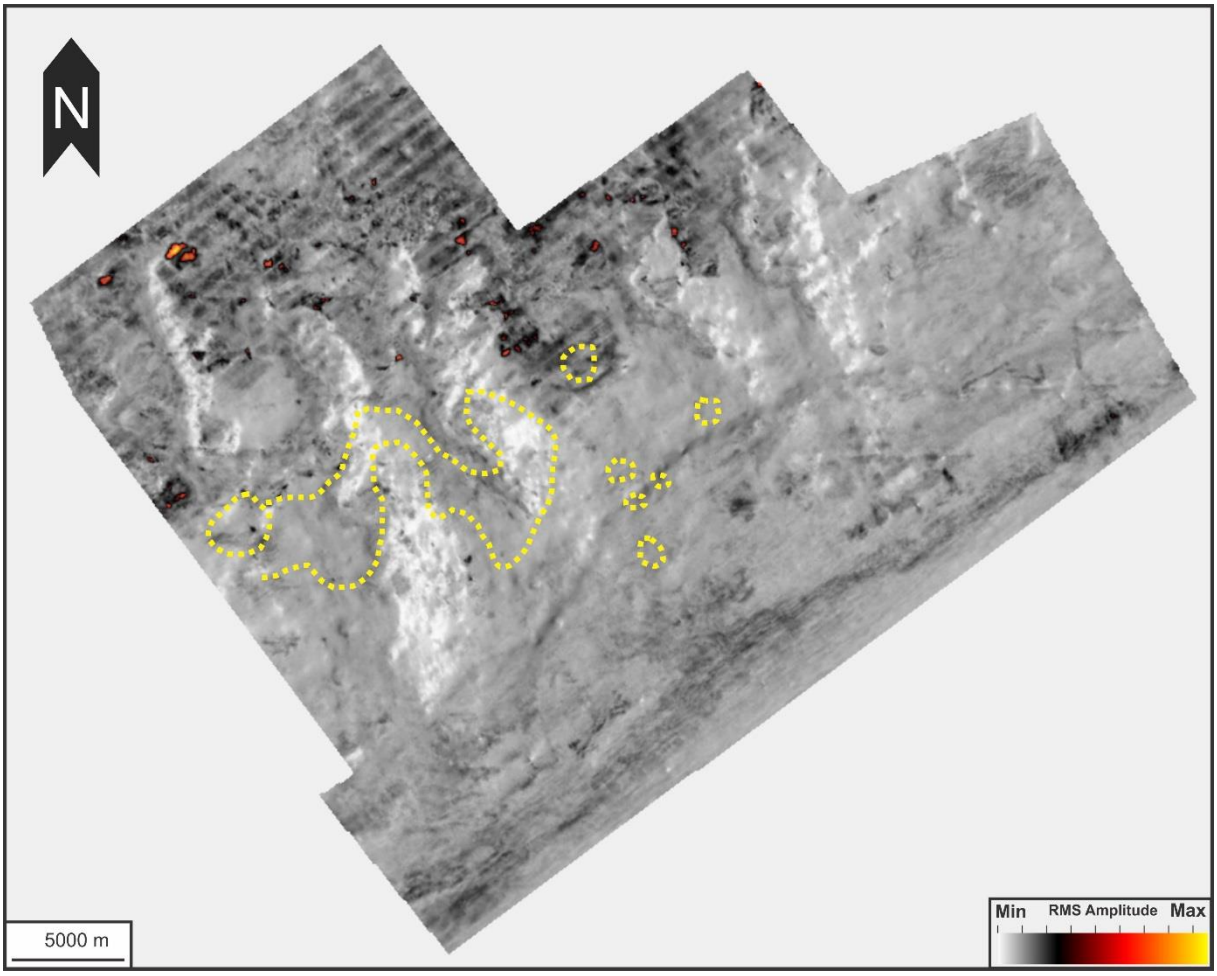

Figure 4-12: RMS amplitude map of S1. The RMS search window is set to 30 above base canyon reflector. Yellow lines illustrates depressions on the seafloor.

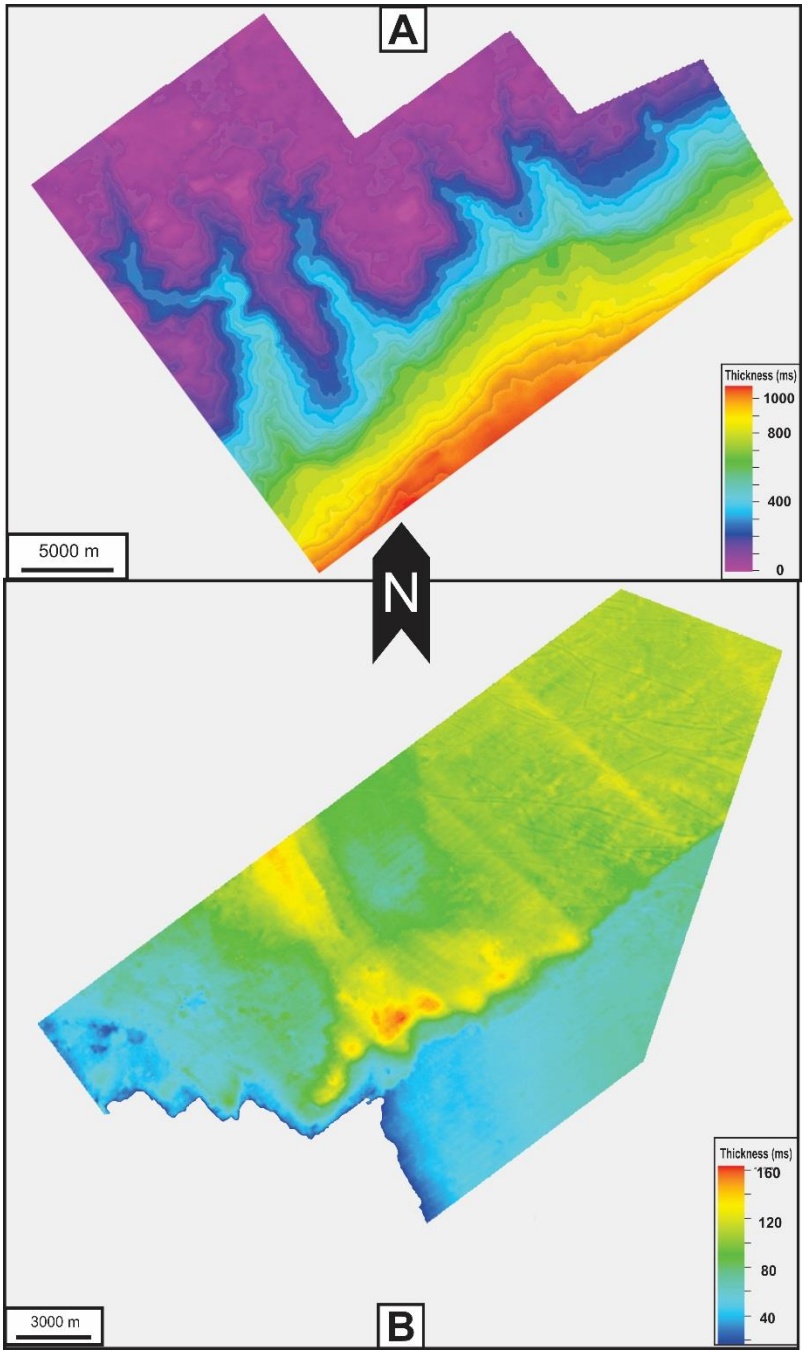

Figure 4-13 ***A:*** *Thickness map of unit S1.* ***B:*** *Thickness map of unit S2. Overview of seismic units are seen in Figure 4-11.*

4.2.3 S2

4.2.3.1 Description

Seismic unit S2 (Figure 4-11 & Figure 4-13) is situated between the URU and seafloor (Figure 4-1). The unit is up to 160 ms TWT thick in the central part of the study area, and about 100 ms TWT thick in the northeastern areas (Figure 4-13). Towards east, the unit displays a wedge geometry. The western and eastern areas generally show very similar patterns with thickness around 40 ms TWT. Thin and somewhat flat areas are found in the northern parts with thickness around 80 ms TWT. Reflection configuration is in general discontinuous, with various amplitude strengths.

High-amplitude areas is mostly seen in S2 (Figure 4-14) in the north and northeast of the survey. Reflections is highly distorted and weak within S2 in areas close to amplitude peaks. Signs of fluid migration is present and related to areas in proximity to high-amplitudes and often correlates with circular seafloor depressions (Figure 4-7 C). Depressions of the URU surface (Figure 4-5) are also in proximity to high amplitude beneath S2 (Figure 4-10 & Figure 4-14).

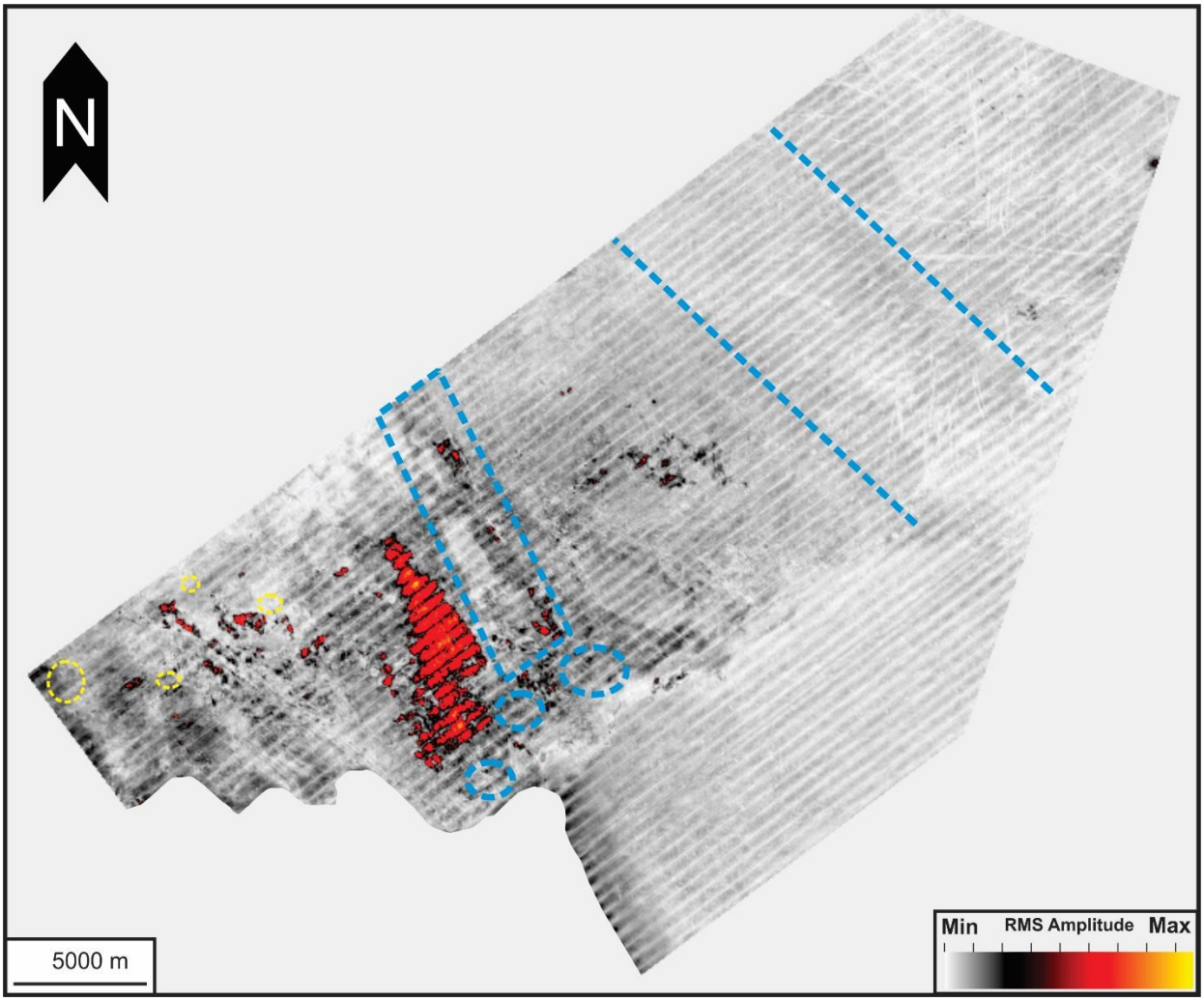

Figure 4-14: RMS amplitude map of seismic unit S2. RMS search window is set to 25 above URU. Yellow lines illustrates depressions of seafloor, whilst blue lines illustrates URU depressions.

4.2.3.2 Interpretation

The wedge in the eastern part is likely the result of an advancing glacier, as reconstructed by (Winsborrow et al., 2010).

The high-amplitude area in the middle of the S2 unit (Figure 4-10 & Figure 4-14) is likely related to the former ice streams in the area by removing unconsolidated sediments and leaving resistant rock. The amplitude anomalies are explained through these lithological changes (change in acoustic impedance), as this area displays the same direction as the depression of the URU surface seen in Figure 4-5. Other high-amplitude anomalies seen in S2 is likely linked with fluid migration, which can be explained by the correlation of fluid related seafloor depressions (Figure 4-7 C).

5. Discussion

The results and observations from the stratigraphy chapter will be further used to explain and document how the seabed and URU depressions within Ingøydjupet are formed, and how the amplitude anomalies found within SG9803 are related to these depressions. Mechanisms related to fluid migration will also be further analyzed and integrated with the results.

5.1 Shallow gas accumulations on the southeastern Loppa High

The acoustically masked areas observed in the result chapter yields valuable information about accumulation, trapping and migration pathways. Fluid flow through marine sediments is a dynamic process, as fluid migration is associated with excess pore-fluid pressure, uplift and erosion, dissociation of gas hydrates, and hydrocarbon generation, leakage from deep and shallow source rocks and reservoirs (Vadakkepuliyambatta et al., 2013).

5.1.1 Source and migration of fluids

Zones of acoustic masking and/or acoustic distortions is common beneath the canyon reflector in seismic unit S0 (Figure 4-10). The deteriorated seismic signal suggest that this is associated with gas chimneys. This indicates that the chimneys seen in the study area represents leakage pathways (Figure 5-1). However, permeability is seldom the same in all directions within a rock and vertical permeability is generally far lower than permeability horizontally to the bedding (Selley, 1998). Thus, migration takes place in all directions, but S0 is probably more permeable than S1, causing the migration paths observed within S0 and along the canyon flanks (Figure 5-1). Faults are a common feature within the Snadd formation and in areas where acoustic masking occur, and can be seen all over the SG9803 survey (in both areas beneath the canyons and areas beneath the URU). Migration linked with shallow faults are likely a contributor some of the shallow gas and accumulations seen (Figure 5-2).

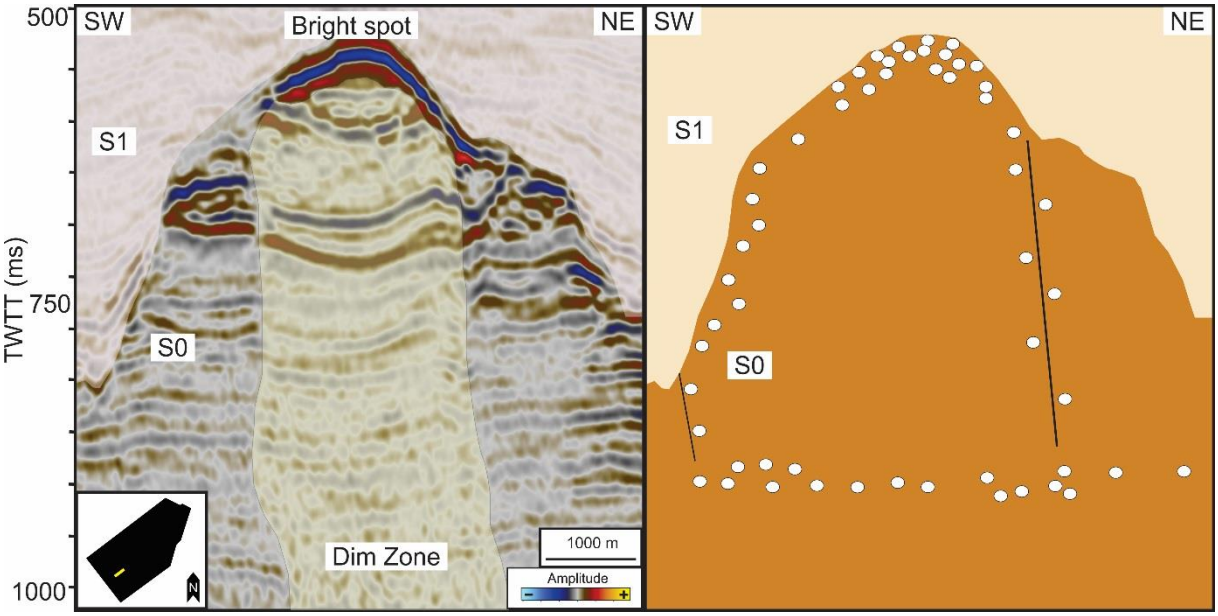

Figure 5-1: Concept model of fluid flow within canyon #2 in seismic unit S0. The dim zone (shaded yellow) is an indication of fluid accumulation and is terminated as a high amplitude bright spot.

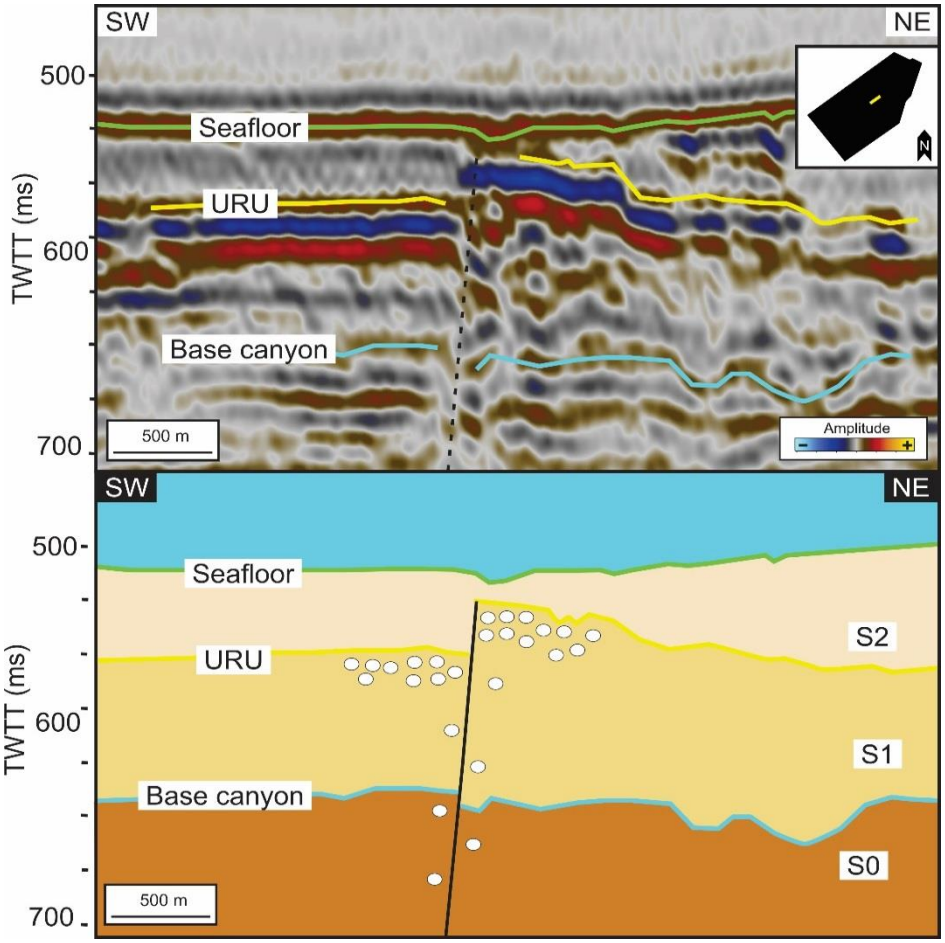

Figure 5-2: Concept model of shallow fault related fluid migration within the survey. The fault plane is related to acoustic masking, which is terminated as a high amplitude area beneath the URU. This suggest that the URU is impermeable in this area causing accumulation of fluids.

5.1.2 Distribution of shallow gas

High amplitude anomalies linked with accumulation of shallow gas are differently distributed due to the different nature seen within the seismic units. As observed in seismic unit S0, the anomalies are mostly situated in the canyon ridges and along the canyon flanks (Figure 4-10). These observations suggests that accumulation within S0 is caused by the different permeability compared to S1.

As seen in the RMS amplitude maps (Figure 4-10, Figure 4-12, Figure 4-14), few high amplitude areas can be seen above the URU, or within S2. High-amplitude areas are mostly situated beneath the URU (Figure 5-2). This suggests that S2 has a low permeability and traps ascending gas in most of the survey, although anomalies are observed in the western parts (Figure 4-13). In the southwestern areas where the URU is not present, it is observed a very different topography on the seafloor (Figure 4-8). This correlation strongly suggests that the absence of URU leads to gas seepage to the water column and different properties of the seabed, or S2, which further causes the large depressions observed (Figure 5-3). The depressions will be discussed later.

However, there are anomalies found within S2 (above the URU) (Figure 4-14), which may be linked with faulting and/or fracturing due to pressure build up. These anomalies are mostly found in the western parts of the survey, where the URU seems to have an impact on S0 (as an impermeable barrier altering pathways), and related to the depressions seen in the seabed where S2 is present (Figure 4-7 & Figure 5-4).

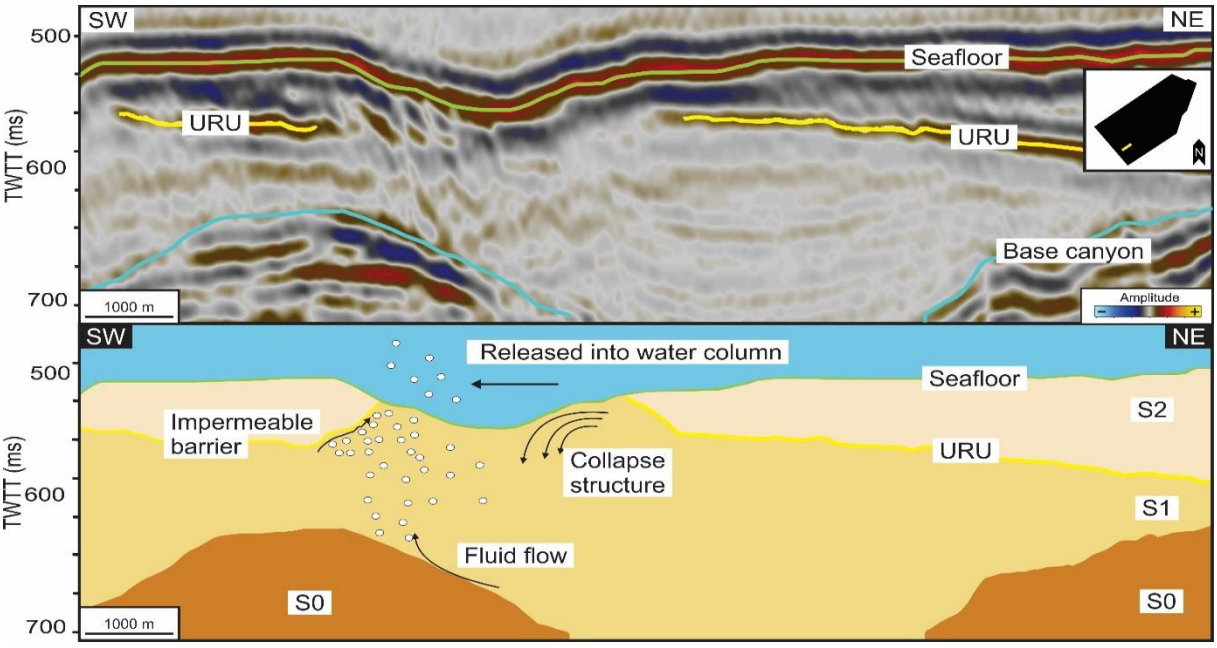

Figure 5-3: Concept model of fluid migration related to the presence of the upper regional unconformity (URU). The model is based on the depression seen as the collapse structure seen in (Figure 4-7).

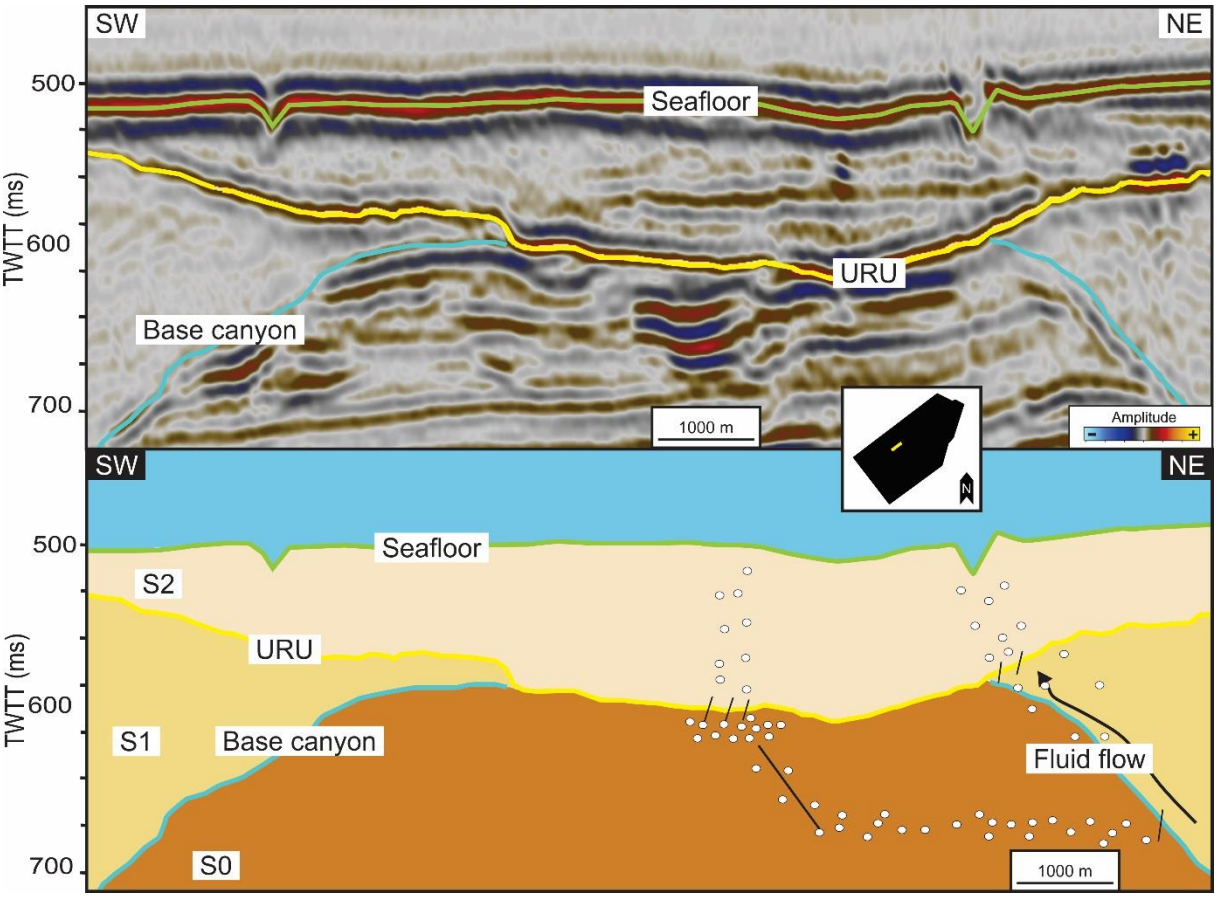

Figure 5-4: Concept model of depressions observed above the URU. Fluid migration is seen as distorted seismic on the right side. It is hard to say if migration takes place from S0 to S2, but accumulation can be observed as a high amplitude area beneath the URU. The depressions in the seafloor are likely pockmarks.

5.2 Large collapse features and pockmarks on the seabed and URU

Several depressions are observed and identified throughout the study, and appears on both the seafloor and URU. These occurs where fast-flowing glaciers have eroded the surface in Area III (Figure 4-8), and where sub-surface fluid migration is observed as high-amplitude areas, which is mostly related to base canyon surface migration (S0 & S1) (Figure 4-10), and the associated distorted seismic. This suggests that they are caused by underlying fluid migration and gas expulsion within S0 and S1, as seen in the seismic data. The correlation of canyon related fluid migration and seabed depressions is shown more detailed in Figure 5-5. These depressions are therefore very likely related to shallow gas, as there is profound evidence of migration along the canyon flanks before accumulating in the crests. The depressions varies greatly in size and some of the larger ones cuts into the lithified bedrock. Their large size is likely credited to large amounts of fluids freed instantly by glacial related gas expansion later explained (Figure 5-6). The remaining URU surface (seismic unit S2) in the area is likely related to distribution and shape of depressions. This observation can be seen in (Figure 5-3), where small parts of impermeable barrier remains, thereby altering the distribution of seafloor depressions, as seafloor depressions are smaller where S2 is present. However, large circular depressions situated in the central parts on the URU surface (Figure 4-5) strongly correlates with observed seafloor depressions, suggesting the same formational mechanisms caused by eruption and seepage of shallow gas (Figure 5-5).

Seafloor Area II (Figure 4-7) contains smaller circular to semi-circular depressions identified as pockmarks. As most pockmarks develop in areas where seafloor sediments are fine-grained, suggests that less glacial related erosion have taken place in these areas. The distribution of smaller depressions further seems to correlate with the absence of the URU, or the S2 unit and the fluid migration pathways previously discussed. Depressions seen in Area II are likely caused by shallow fault migration within S2. The smaller circular depressions observed on the southeastern URU surface (Figure 4-4) are likely caused by artefacts, and thus not paleo pockmarks or linked with fluid migration.

The seabed depressions have previously been interpreted as a tunnel valley formed by sub-glacial melt-water (Andreassen et al., 2008). However, depressions in the SW Barents Sea are often related to expulsion of shallow gas and Ingøydjupet has numerous fluid related depressions, e.g. (Vadakkepuliyambatta et al., 2013; Rise et al., 2015). Hence, there is little doubt that ascending shallow gas affects the formational mechanisms of these collapse structures and depressions (Figure 5-5). Similar crater structures are observed in Bjørnøyrenna, a major trough in the Barents Sea, which shares the same properties as Ingøydjupet Trough. These crater structures have been interpreted not to

originate from sub-glacial melt-water, as these depressions were incompatible with the distinct appearance and patterns related to sub-glacial melt water and formed after grounded ice retreated from that area. These studies concluded with a process related to shallow gas or gas hydrates (Solheim & Elverhøi, 1985; Solheim, 1991; Solheim & Elverhøi, 1993).

The most widely accepted explanation of depressions related to seafloor gas seepage are from both thermogenic sources and biological breakdown of organic matter (Hovland & Judd, 1988; Judd, 2004). As for this area, biogenic sources may probably be excluded, as organic matter in late glacial depositions seldom exceed 1-2%, which is to scarce to create such depressions (Solheim & Elverhøi, 1985). Gas of thermogenic origins are thus the likely cause of the observed depressions in the study area. Seepage are known to differ in both as controlled seepage and as explosive and sudden expulsion, creating depressions of different sizes. The ascending fluids are then distributed in the surrounding water column (Hovland & Judd, 1988; Judd & Hovland, 2007).

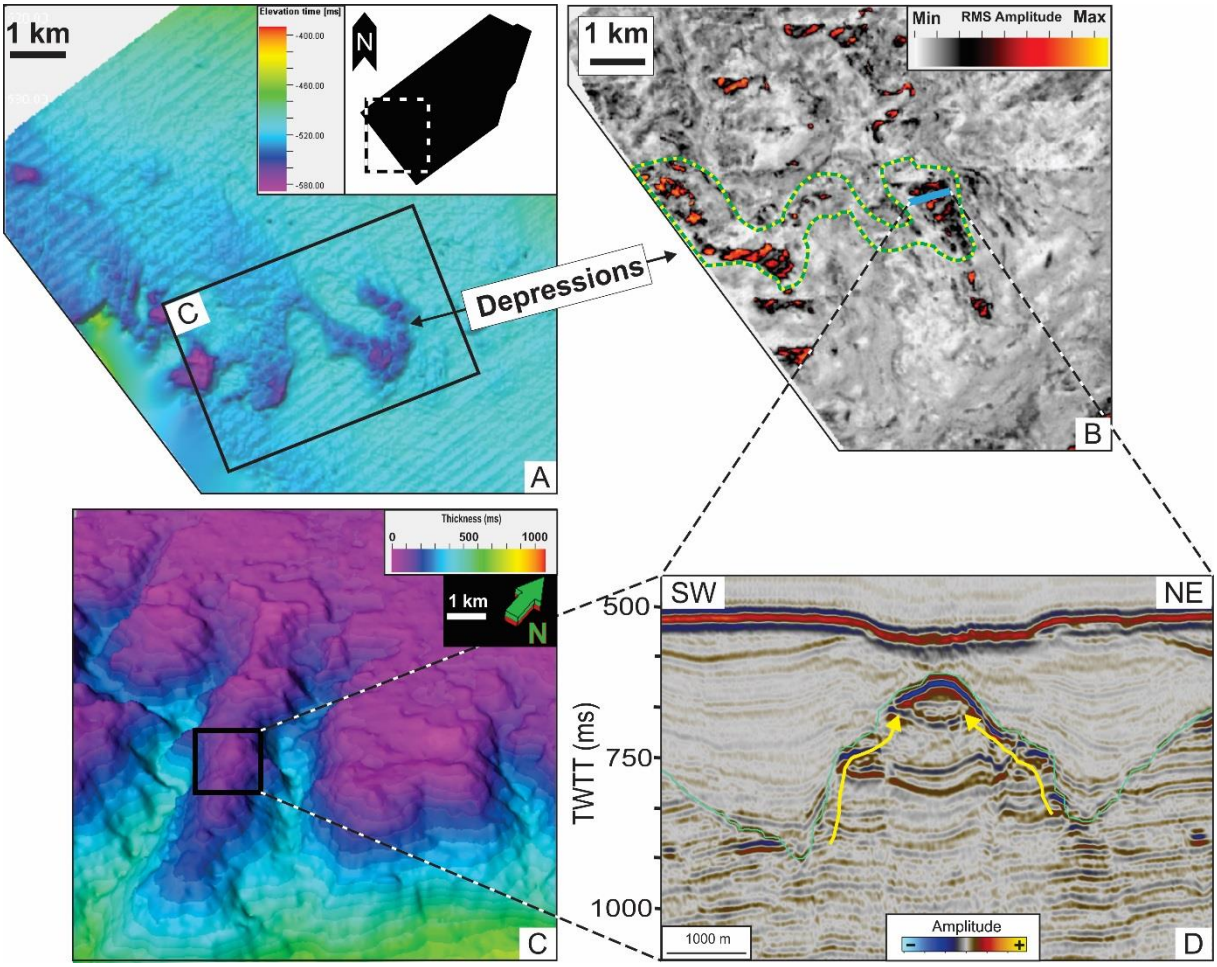

Figure 5-5: The relationship between sub-surface high-amplitudes, buried canyons and seafloor depressions. ***A:*** *Map of the seafloor displaying depressions (10x vertical exaggeration).* ***B:*** *RMS amplitude map of the canyon ridges within seismic unit S0. Its correlation of seafloor depressions is illustrated as the yellow/green dotted line (RMS search window set to 25 ms below the base canyon reflector).* ***C:*** *A time thickness map of seismic unit S1 (stratigraphically beneath the seafloor, as S2 is not present in this area). As accumulation takes place in the crests, the overlaying depressions are influenced by the extent of the canyons.* ***D****: Seismic section of a high-amplitude area of a canyon crest. Yellow arrows displays the fluid migration along canyon flanks. Notice that the depression is situated directly above fluid accumulation.*

5.3 Historical evolution and its impact on the observed depressions

Regional fluid expulsion is severely affected by erosion and deglaciation, as sub-surface gas expands due to retreating glaciers through glacial isostatic adjustment. This implies that fluid expulsion likely happened during the Quaternary. The expansion of gas eventually caused massive amounts of pressure to build up, which subsequently caused violent eruptions and the collapse features and pockmarks seen within the area. This is explained in more detail in Figure 5-6. Erosion and deglaciation is well known to facilitate fluid migration and expulsion in the SW Barents Sea, e.g. (Chand et al., 2012).

As today's seafloor topography differs, fluid migration will subsequently do so as well. Seafloor Area I & II consists of moraine depositions, whilst area III displays erosional features (Figure 4-6 - Figure 4-8). The moraine depositions (Area I & II) in Ingøydjupet consists of Nordkappbanken, a sedimentary wedge, to the east, and Bjørnøyrenna end moraine zone to the north. These depositional environments prevents fluids to reach the seabed and form depressions, as sediment cover is generally thick. In Area III, however, the eroding ice streams have altered the topography by removing top layers (seismic unit S2), which influences the presence of gas and migration pathways, as seen in the concept model in Figure 5-6.

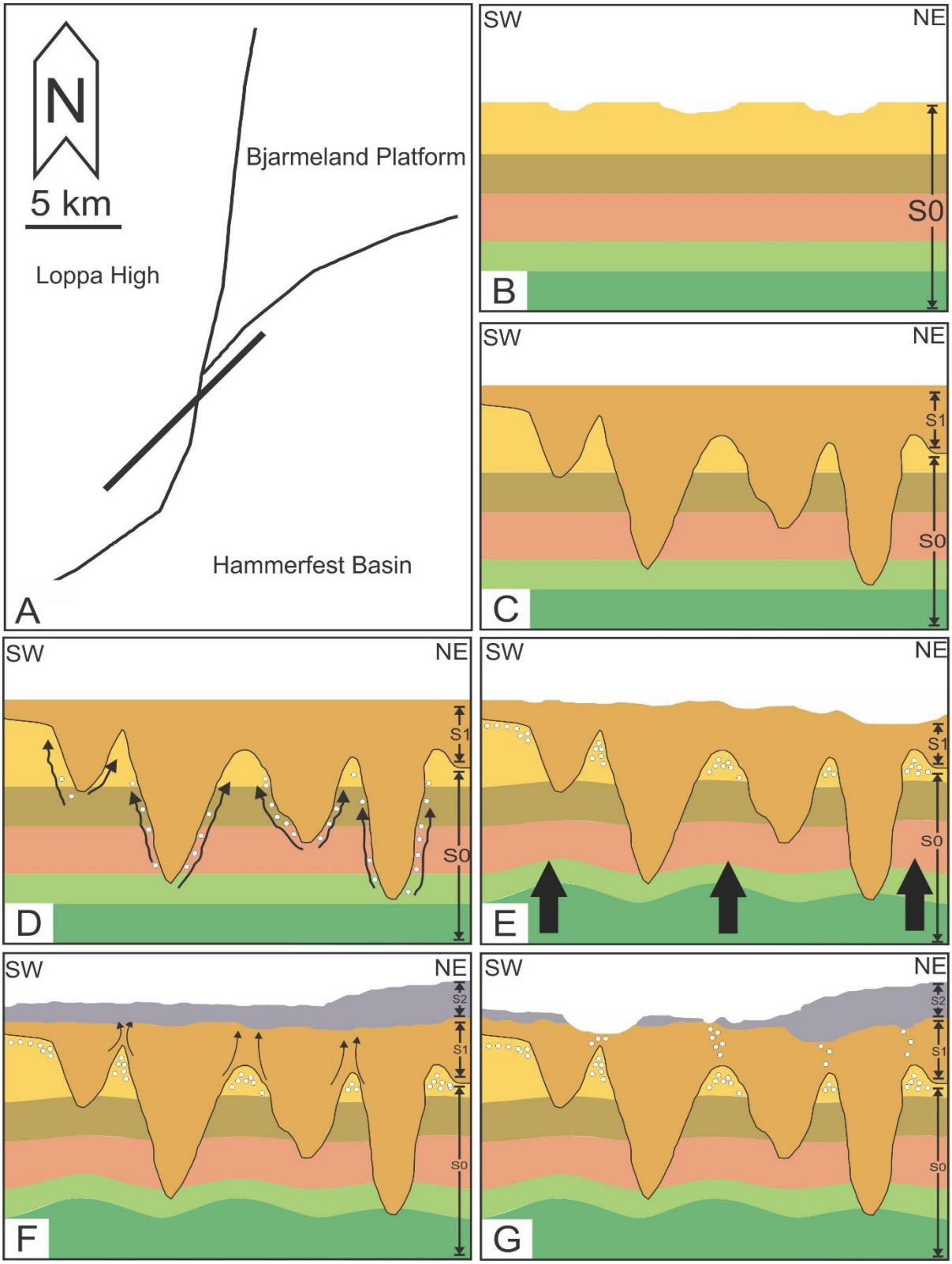

Figure 5-6: ***A:*** *Overview of the area with a conceptual profile.* ***B:*** *Jurassic and Triassic strata (unit S0) with the initial erosion and uplift of the Loppa High.* ***C:*** *Infill of Cretaceous and Cenozoic sediments creating unit S1.* ***D:*** *Fluid migration and accumulation takes place for an unknown period.* ***E:*** *Quaternary glacial erosion takes place, eroding top sediments of unit S1 and creates unit S2. As glaciers retreat, isostatic rebound causes regional uplift.* ***F:*** *The uplift causes the gas to expand, which builds up enormous pressure.* ***G:*** *The pressure reaches critical values and eruptive mechanisms causes the depressions seen on both the URU and the surface.*

6. Conclusion

- Interpretation and the use of geophysical attributes in the 3D seismic survey SG9803 has made it possible to map out shallow high-amplitude anomalies and infer the distribution of shallow gas in the Loppa High, SW Barents Sea.
- The study area contains numerous acoustically masked zones and high-amplitude associated with fluid migration and accumulation.
- High-amplitude areas are frequently associated with canyon crests, suggesting migration along the flanks and faults with accumulation in the crests.
- The seabed depressions on the southeastern rim of the Loppa High appears to have a strong correlation with the gas accumulations observed at the canyon crests. These depressions are therefore most likely related to shallow gas, and not formed by subglacial melt-water as previously interpreted.
- Uplift and erosion appears to be a major contributor to fluid migration, as it affects sub-surface expansion of shallow gas. As the shallow gas expands, pressure builds up and violent eruptions and seepage takes place. Fluid related depressions are also found on the URU.
- The size and distribution of depressions are further related to glacial erosion and depositions. In areas where the sediment cover is thin, fluid related depressions are abundant, as seismic unit S2 is not present. There are no signs of fluid related depressions on the northern and northeastern parts of the study area where the sediment cover is generally thicker.

7. References

Aagaard-Sørensen, S., Husum, K., Hald, M. & Knies, J., 2010. Paleoceanographic development in the SW barents sea during the Late Weichselian-Early Holocene transition. *Quaternary Science reviews,* Volume 97, pp. 3442-3456.

Andreassen, 2009. *Marine Geophysics lecture notes,* :UIT.

Andreassen, K., Laberg, J. S. & Vorren, T., 2008. Seafloor geomorphology of the SW Barents Sea and its glaci-dynamic implications. *ScienceDirect.*

Andreassen, K., Nilssen, E. G. & Ødegaard, C. M., 2007. Analysis of shallow gas and fluid migration within the Plio-Pleistocene sedimentary succession of the SW Barents Sea continental margin using 3D seismic data.

Badley, E. M., 1985. *Practical Seismic Interpretation*.:International Human Resources development Corporation.

Bear, J., 1972. *Dynamics of Fluids in Porous Media.* :Dover.

Berndt, C., 2005. Focused fluid flow in passive continental margins. *Triennial Issue: 'Astronomy and earth science' ,* 363(1837), pp. 2855-2871.

Bugge, T. et al., 1995. The Upper Palaeozoic succession on the Finnmark Platform, Barents Sea. *Norsk Geologisk Tidsskrift,* Volume 75, pp. 3-30.

Cartwright, J., Huuse, M. & Apling, A., 2007. Seal bypass systems. *American Association of Petroleum Geologists Bulletin,* Volume 91, pp. 1141-1166.

Castagna, J., Batzle, M. & Kan, T., 1993. Rock physics—the link between rock properties and AVO response. *Theory and Practice of AVO Analysis,* Volume 8, pp. 124-157.

Chand, S. et al., 2009. Pockmark-like depressions near the Goliat hydrocarbon field, Barents Sea: Moprhology and genesis. *Marine and Petroleum Geology,* Volume 26, pp. 1035-1042.

Chand, S. et al., 2012. Multiple eposodes of fluid flow in the SW Barents Sea evidenced by gas falres, pockmarks and gas hydrate accumulation. *Earth and Planetary Science Letters,* pp. 305-314.

Chistyakova, N. et al., 2010. Reconstruction of the postglacial environments in the southwestern Barents Sea based on foraminiferal assemblages. *Oceanology,* Volume 50, pp. 573-581.

Chistyakova, N. et al., 2010. Reconstruction of the postglacial environments in the SW Barents Sea based on foraminiferal assemblages. *Oceanology,* Volume 50, pp. 573-581.

Clark, S. et al., 2014. Southwest Barents Sea rift basin evolution:comparing results from backstripping and time-forward modelling. *Basin Research,* 26(4), pp. 550-566.

Deibert, J. E. et al., 2003. Eocene clinoform growth in front of a storm-wave-dominated shelf, Central Basin, Spitsbergen: nosignificant sand delivery to deepwater areas.. *Journal of Sedimentary Research,* Volume 73, pp. 546-558.

Doré, A. & Jensen, L., 1996. The impact of late Cenozoic upplift and erosion on hydrocarbon exploration: offshore Norway and some other uplifted basins.. *Global and Planetary Change,* Volume 12, pp. 415-436.

Doré, W. P., 1995. Barents Sea Geology, petroleum resources and commercial potential. *Arctic,* Volume 48, pp. 207-221.

Faleide, J., Gudlaugsson, T. & Jacquart, G., 1984. Evolution of the western Barents Sea. *Marine and petroleum geology,* Volume 1, pp. 123-150.

Faleide, J. I., Bjørlykke, K. & Gabrielsen, R., 2015. Geology of the Norwegian Continental Shelf. *Petroleum Geoscience,* p. Chapter 25.

Faleide, J. I. et al., 1996. Late Ceozoic evolution of the western Barents Sea - Svalbard continental margin. *Global and Planetary Change,* Volume 12.

Faleide, J., Vågnes, E. & Gudlaugsson, S., 1993. Late Mesozoic-Cenozoic evolution of the south-western Barents Sea in a regional rift-shear tectonic setting. *Marine and PEtroleum geology,* Volume 10, pp. 186-214.

Gabrielsen, G., Færseth, R. & Jensen, L., 1990. Structural Elements of the Norwegian Continental Shelf. Pt. 1. The Barents Sea Region. *NPD,* pp. 2-47.

Gudlaugsson, S., Faleide, J., Johansen, S. & Breivik, A., 1998. Late Palaeozoic structural development of the SW Barents Sea. *Marine and petroleum geology,* Volume 15, pp. 73-102.

Guzzetta, G. & Cinquegrana, R., 1987. Fluid tectonic: a little appreciated facet of buoyancy tectonics. *Tectonophysics,* 139(3-4), pp. 321-324.

Hald, M., Danielsen, T. & Lorentzen, S., 1989. Late Pleistocene-Holocene Benthic foraminiferal distribution in the southwestern Barents sea - paleoenvironmental implications. *Boreas,* Volume 18, pp. 367-388.

Halland, E. et al., 2013. CO2 Storage atlas - Barents Sea. *Geological description of the Barents Sea,* pp. 22-38.

Henriksen, E., Bjørnseth, H. M. & K, H. T., 2011 b. Uplift and erosion of the greter Barebts Sea: impact on prospectivity and petroleum systems. *Geological Society, London, Memoirs,* pp. 271-281.

Henriksen, E., E, R. A. & B, L. G., 2011. Tectonostratigraphy of the greater Barents Sea: implications for petroleum systems. *Geological Society, London, Memoirs,* Volume 35, pp. 163-195.

Hooper, E. C. D., 1991. Fluid migration along growth faults in compacting sediments. *Journal of petroleum geology,* Volume 14, pp. 161-180.

Hovland, M. & Judd, A., 1988. Seabed Pockmarks and Seepages. Impact on Geology, Biology and Marine Environment. *Geological Magazine,* 127(1), pp. 85-86.

Johannesen, H., 2006. Holocene climate variability in the norwegian current and north cape current inferred from benthic stable isotope records. *MSc thesis, University of Tromsø,* p. 90.

Judd, A., 2004. Natural seabed gas seeps as sources of atmospheric methane. *Environmental Geology,* Volume 46, pp. 988-996.

Judd, A. & Hovland, M., 2007. *Seabed Fluid Flow - Impact of geology, biology and the marine environment.*

Knipe, R. J., 1992. Faulting processes and fault seal. *Structural and tectonic modelling and its application to petroleum geology,* Volume 1, pp. 325-342.

Laberg, J. S., Andreassen, K. & Vorren, T., 2012. Late Cenozoic erosion of the high-latitude southwestern Barents Sea shelf revisited. *Geological Society of America Bulletin,* Volume 124, pp. 77-88.

Landvik, J. Y. et al., 1998. The last glacial maximum of Svalbard and the Barents Sea area: ice sheet extend and configuration. *Quaternary Science REviews,* Volume 17, pp. 43-75.

Larssen, G. B. E. G. H. L. B. K. S. E. et al., 2002. Upper Palaeozoic lithostratigraphy of the Southern Norwegian Barents Sea. *NPD Bulletin,* Volume 9, p. 69.

Linjordet, A. & Grung, R., 1992. The Jurassic Snøhvit Gas Field, Hammerfest Basin, Offshore northern Norway. *American Association of Petroleum Geologists Memoir,* Volume 54, pp. 349-370.

Løseth, H., Gading, M. & Wensaas, L., 2008. Hydrocarbon leakage interpreted on seismic data. *Marine and petroleum geology,* Volume 26, pp. 1304-1319.

Midtbø, M., 2000. Studier av kenozoiske erosjonsflater i det sørvestlige Barentshavet ved bruk av tredimensjonale seismiske data. *Hovedfagsoppgave i marin geologi.*

NPD, 2008. *Oljedirektoratet.* [Online]
Available at: http://www.npd.no/no/Nyheter/Resultat-av-leteboring/2008/Gassfunn-i-Barentshavet---722211-1/
[Accessed 19 3 2016].

NPD, 2016. *NPD Factpages.* [Online]
Available at: http://factpages.npd.no/FactPages/default.aspx?nav1=survey&nav2=PageView|Finished|1998&nav3=3940&culture=en
[Accessed 19 3 2016].

Nyland, B. et al., 1992. *Tertiary Uplift and Erosion in the Barents Sea; Magnitude, Timing and Consequences.* s.l.:s.n.

Ohm, S. E., Karlsen, D. & Austion, T. J. F., 2008. Geochemically driven exploration models in uplifted areas: Examples from the Norwegian Barents Sea. *AAPG Bulletin,* 92(9), pp. 1191-1223.

Rafaelsen, B., 2006. Seismic resolution (and frequency filtering).

Reemst, P. & Cloetingh, S., 1994. Tectonostratigraphic modelling of Cenozoic uplift and erosion in the SW Barents Sea. *Marine and Petroleum Geology,* 11(4).

Riis, F., Vollset, J. & M, S., 1986. Tectonic development of the western margin of the Barents Sea and adjacent areas. *AAPG Memoirs,* pp. 661-676.

Rise, L., Bellec, V., Chand, S. & Bøe, R., 2015. Pockmarks in the southwestern Barents Sea and Finnmark fjords. *Norwegian Journal of geology.*

Ryseth, A. et al., 2003. Cenozoic stratigraphy and evolution of the Sørvestsnaget Basin, southwestern Barents Sea. *Norwegian Journal of Geology,* Volume 83, pp. 107-130.

Röthlisberger, H., 1972. Water pressure in intra- and subglacial channels. *Journal of Glaciology,* 11(62), pp. 177-203.

Selley, R., 1998. *Elements of Petroleum geology.* second edition ed. s.l.:Academic Press.

Smelror, M., Petrov, O., Larssen, B. & Werner, S., 2009. *Geological history of the Barents Sea.* s.l.:NGU.

Solheim, A., 1991. The depositional environment of surging sub-polar tidewater glaciers: A case study of the morphology, sedimentation and sediment porperties in a surge-affected marine basin outside Nordaustlandet, Northern Barents Sea. *Norsk Polarinstitutt Skrifter,* Volume 194, p. 97.

Solheim, A. & Elverhøi, A., 1985. A pockmark field in the Central Barents Sea; gas from a petrogenic source?. *Polar reasearch,* Volume 3, pp. 11-19.

Solheim, A. & Elverhøi, A., 1993. Gas-related seafloor craters in the Barents Sea. *Geo-Marine Letters,* Volume 13, pp. 235-243.

Statoil, 1986. *Completion report well 7121/4-1,*

Steel, R. & Worsley, D., 1984. Svalbards post-caledonian strata - an atlas of sedimentational patterns and paleogeographic evolution. *Petroleum Geology of the north European Margin,* pp. 109-135.

Vadakkepuliyambatta, S., Bunz, S., Mienert, J. & Chand, S., 2013. Distribution of subsurface fluid-flow systems in the SW Barents Sea. *Marine and Petroleum Geology,* Volume 43, pp. 208-221.

Veeken, P., 2007. Seismic Stratigraphy, basin analysis and reservoir characterisation. *Handbook in Seismic Exploration,* pp. 111-134.

Vorren, T. & Mangerud, J., 2006. Istider kommer og går. Sein pliocent og pleistocen. *Landet blir til - Norges geologi,* pp. 478-531.

Vorren, T. O. & Kristoffersen, Y., 1986. Late Quaternary glaciation in the south-western Barents Sea. *Quaternary Science & Glaciology,* 15(1), pp. 51-59.

Vorren, T., Richardsen, G. & Knutsen, S. M., 1991. Cenozoic erosion and sedimentation in the western Barents Sea. *Marine and Petroleum Geology,* 8(3), p. 317–340.

Whitaker, S., 1986. Flow in porous media I: A theoretical derivation of Darcy's law. *Transport in Porous Media,* 1(1), pp. 3-25.

Winsborrow, M. C., Andreassen, K., Corner, G. D. & Laberg, J. S., 2010. Deglaciation of a marine-based ice sheet: Late Weichselian paleo-ice dynamics and retreat in the southern Barents Sea reconstructed from onshore and offshore glacial geomorphology. *Quaternary Science Reviews,* Volume 29, pp. 424-442.

Wiprut, D. & Zoback, M. D., 2000. Fault reactivation and fluid flow along a previosly dormant normal fault in the northern North Sea. *Geology,* Volume 28, pp. 595-698.

Worsely, D., R, J. & Kristensen, S., 1988. The Mesozoic and Cenozoic succession of Tromsøflaket. In: A Lithostratigraphic Scheme for the Mesozoic and Cenozoic Succession Offshore Mid- and Northern Norway. *NPD Bulletin ,* Volume 4, pp. 42-65.

Worsley, D., 2008. The post-Caledonian development of Svalbard and the western Barents Sea. *Issue Polar Research,* 27(3), pp. 298-317.

Yilmaz, Ö., 2001. *Seismic Data Analysis.*

Zaborska, A. et al., 2008. Recent sediment accumulation rates for the western. *Deep–Sea Research II.*